PHYSICS AT THE Z POLE WITH SLD

Stéphane Willocq*

Stanford Linear Accelerator Center

Stanford University, Stanford, California 94309

Representing the SLD Collaboration**

Stanford Linear Accelerator Center, Stanford University, Stanford, CA 94309

ABSTRACT

We review recent results from a wide physics program in polarized e^+e^- interactions at the SLC performed by the SLD experiment. Unique and precise measurements of the electroweak parameters A_e, A_b, A_c, and R_b provide valuable constraints on the Standard Model. The excellent 3-D vertexing capabilities of SLD are further exploited to extract precise B^+ and B_d^0 lifetimes, as well as measurements of the time evolution of $B_d^0 - \overline{B_d^0}$ mixing. Finally, the unique capabilities of the SLC/SLD are used to test QCD in new ways. We present results on general properties of particle production in light, c, and b quark events, as well as the first observation of leading particle production in light-quark hemispheres.

DISCLAIMER

Portions of this document may be illegible
in electronic image products.   Images are
produced from the best available original
document.

DISCLAIMER

where $\cos\theta$ is the cosine of the angle between the final state fermion f and the incident electron directions, P_e is the electron beam longitudinal polarization, and A_e and A_f are the asymmetry parameters for the initial and final state fermions, respectively. The asymmetry parameter for a given fermion represents the extent of parity violation at the $Z^0 \to f\bar{f}$ vertex and is defined as

$$A_f = \frac{2 g_V g_A}{g_V^2 + g_A^2} = \frac{g_L^2 - g_R^2}{g_L^2 + g_R^2},$$
(5)

with the left- and right-handed coupling constants $g_L = \frac{1}{2}(g_V + g_A)$ and $g_R = \frac{1}{2}(g_V - g_A)$.

The presence of parity violation introduces a forward-backward asymmetry $A_f^{FB} = \frac{\sigma_f^F - \sigma_f^B}{\sigma_f^F + \sigma_f^B}$ which is equal to $\frac{3}{4} A_e A_f$. At the SLC, the electron beam polarization allows a polarized forward-backward asymmetry to be measured

$$\tilde{A}_f^{FB} = \frac{\left[\sigma_f^F - \sigma_f^B\right]^{\text{left}} - \left[\sigma_f^F - \sigma_f^B\right]^{\text{right}}}{\left[\sigma_f^F - \sigma_f^B\right]^{\text{left}} + \left[\sigma_f^F - \sigma_f^B\right]^{\text{right}}} = \frac{3}{4} P_e A_f.$$
(6)

The latter asymmetry provides a *direct* measurement of A_f and yields a statistical enhancement factor of $(P_e/A_e)^2$ over the unpolarized forward-backward asymmetry. This relative enhancement is roughly equivalent to a statistical gain of 25 at the SLC.

Another interesting asymmetry is the left-right cross-section asymmetry

$$A_{LR}^0 = \frac{\sigma_L - \sigma_R}{\sigma_L + \sigma_R} = A_e,$$
(7)

which yields a direct measurement of the coupling between the Z^0 and the $e^+ e^-$ initial state.

Measurements of partial Z^0 decay widths also provide information regarding the $Z^0 \to f\bar{f}$ couplings. The ratio between the partial decay width into a particular final state fermion and that into any hadron is sensitive to the left- and right-handed coupling constants g_L and g_R of fermion f

$$R_f = \frac{\Gamma(Z \to f\bar{f})}{\Gamma(Z \to \text{hadrons})} \propto g_L^2 + g_R^2 .$$
(8)

Precise measurements of the asymmetry parameters A_f and the partial widths R_f can probe the effect of radiative corrections to the Z^0 propagator or to the $Zf\bar{f}$ vertex. Since the radiative corrections depend on the top and Higgs masses,
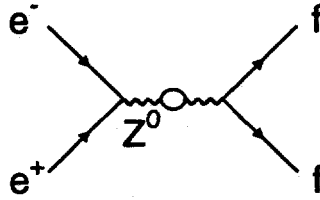
3

Figure 1: Feynman diagram showing radiative corrections affecting the Z^0 propagator.

precise electroweak measurements can measure or constrain these quantities. Furthermore, such measurements also are sensitive to physics beyond the SM. It is important to measure A_f and R_f for individual fermions since the coupling strengths differ due to differences in electric charge and weak isospin as indicated in Eqs. (2) and (3). Vacuum polarization corrections (Fig. 1) affect the value of $\sin^2 \theta_W^{eff}$ which is most precisely measured by the left-right asymmetry

$$A_{LR}^0 = A_e = \frac{2\left[1 - 4\sin^2\theta_W^{eff}\right]}{1 + \left[1 - 4\sin^2\theta_W^{eff}\right]^2}. \tag{9}$$

Heavy quark partial widths and asymmetry parameters are most sensitive to vertex corrections (Fig. 2) but with different sensitivity to left- and right-handed coupling constants. In particular, since $g_L^2 \simeq 30\, g_R^2$ for b quarks, R_b is most

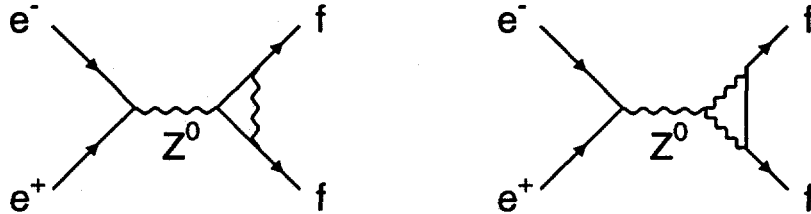Figure 2: Feynman diagrams showing radiative corrections affecting the Z^0 coupling to the final state fermions.

sensitive to deviations in the left-handed coupling between the Z^0 and b quarks, whereas A_b is more sensitive to deviations in the right-handed coupling. Moreover, vertex corrections involving the top quark only affect the left-handed coupling, in the context of the SM.

4

1.1 Polarization at the SLC

As indicated above, many unique and powerful measurements can be performed at the SLC by exploiting the high polarization of the electron beam. Here we only summarize the polarization process; further details may be obtained elsewhere.[1] Electrons are photo-emitted from a strained-lattice GaAs photo-cathode using a Ti-Sapphire laser operating at $\lambda = 849$ nm. The laser beam is circularly polarized to produce either left- or right-handed electrons with maximum polarization near 80%. The polarization sign is randomly flipped from pulse to pulse. The polarization axis is rotated to be vertical for the acceleration and damping phases. At the end of the linac, the polarization axis is rotated by a series of betatron oscillations such that it is longitudinal at the e^+e^- Interaction Point (IP).

The electron beam longitudinal polarization is measured 33 m downstream of the IP by a Compton Polarimeter. A Nd:YAG laser produces circularly polarized photons with energy of 2.33 eV brought to collision with the electron beam. The part of the beam which undergoes Compton scattering is momentum-analyzed with a dipole magnet and detected in a Cherenkov counter. The electron beam polarization is extracted by measuring the asymmetry between parallel and antiparallel configurations of the electron and photon helicities. The polarimeter yields a measurement every three minutes with statistical accuracy near 1%. Two-thirds of the data collected in 1994–95 were dedicated for various calibration checks of the polarimeter. These special runs allow careful control of the systematic uncertainties in the measured polarization. The overall relative systematic uncertainty is estimated to be $\delta P_e/P_e = 1.59\%$ for the 1993 run and 0.67% for the 1994–95 run. The various contributions to this uncertainty are summarized in Table 1; Cherenkov counter linearity is the dominant contribution.

1.2 Left-Right Cross-Section Asymmetry

The measurement of A_{LR} is a simple counting experiment.[2] One needs to count the number of Z^0 produced with left- and right-handed electron beams, and measure the average electron beam polarization. The event selection relies on the Liquid Argon Calorimeter (LAC) and the Central Drift Chamber (CDC) which are also used for the trigger. The selection criteria are chosen to remove two-photon and beam-related background events as well as Z^0 events decaying into e^+e^- final states for which the cross-section includes $t-$channel contributions that dilute

5

Uncertainty	$\delta P_e / P_e$ (%)
Laser polarization	0.20
Detector linearity	0.50
Detector calibration	0.29
Electronic noise	0.20
Compton - IP difference	0.17
Total	0.67

Table 1: Contributions to the polarization systematic uncertainty (1994–95 run).

the left-right asymmetry. The event sample then mostly consists of hadronic Z^0 decays selected with an efficiency of $(89 \pm 1)\%$. In the 1994–95 data, the number of selected events is 52,179 and 41,465 for left- and right-handed electrons respectively. The resulting measured asymmetry is thus $A_m = (N_L - N_R)/(N_L + N_R) = 0.1144 \pm 0.0032(\text{stat})$. To obtain the left-right cross-section asymmetry at the SLC center-of-mass energy of 91.28 GeV, a very small correction $\delta = (0.240 \pm 0.055)\%(\text{syst})$ is applied which takes into account residual contamination in the event sample and slight beam asymmetries. As a result,

$$A_{LR}(91.28 \text{ GeV}) = \frac{A_m}{\langle P_e \rangle}(1 + \delta) = 0.1485 \pm 0.0042(\text{stat}) \pm 0.0010(\text{syst}), \quad (10)$$

where the systematic uncertainty is dominated by our systematic understanding of the beam polarization (see Table 1). Finally, this result is corrected for initial and final state radiation as well as for scaling the result to the Z^0 pole energy:

$$A_{LR}^0 = 0.1512 \pm 0.0042(\text{stat}) \pm 0.0011(\text{syst}), \quad (11)$$

$$\sin^2 \theta_W^{eff} = 0.23100 \pm 0.00054(\text{stat}) \pm 0.00014(\text{syst}). \quad (12)$$

The 1994–95 measurement can be combined with previous measurements from the 1992 and 1993 running periods[3,4] to yield

$$A_{LR}^0 = 0.1543 \pm 0.0039, \quad (13)$$

$$\sin^2 \theta_W^{eff} = 0.23060 \pm 0.00050. \quad (14)$$

The above represents the most precise measurement of $\sin^2 \theta_W^{eff}$ by a single experiment.

Analysis	Asymmetry
$\mu\mu$ and $\tau\tau$	$A_e = 0.148 \pm 0.016$
$\mu\mu$	$A_\mu = 0.102 \pm 0.033$
$\tau\tau$	$A_\tau = 0.190 \pm 0.034$
ee Bhabha (Ref.[6])	$A_e = 0.202 \pm 0.038$
Q_{LR} (Ref.[7])	$A_e = 0.162 \pm 0.043$
A_{LR}	$A_e = 0.1543 \pm 0.0039$
Combined	$A_l = 0.1542 \pm 0.0037$

Table 2: Lepton asymmetry parameter measurements from various analyses.

1.3 Lepton Asymmetries

Further information about $\sin^2 \theta_W^{eff}$ can be obtained from events with Z^0 decaying into a pair of charged leptons (μ or τ). Here, the $\cos\theta$ dependence of the differential cross-section is used (see Eq. 4) and both initial and final state asymmetry parameters can be extracted, i.e., A_e and either A_μ or A_τ. Since the event selection for the left-right asymmetry analysis has poor efficiency for non hadronic Z^0 decays, analyses utilizing $\mu^+\mu^-$ and $\tau^+\tau^-$ final states are statistically independent.

The event selection employs information from the tracking and calorimetry systems to reject $Z^0 \to e^+e^-$, $Z^0 \to$ hadrons, and two-photon events. Using data from 1993 through 1995, a total of 3,788 events is selected in the $\mu^+\mu^-$ analysis and 3,748 events in the $\tau^+\tau^-$ analysis with respective efficiencies of 95% and 89%. The main background to the $\mu^+\mu^-$ sample originates from $\tau^+\tau^-$ events (0.4%), whereas the background to the $\tau^+\tau^-$ sample comes mainly from Z^0 decays into $\mu^+\mu^-$ (4%) and e^+e^- (1%).

The preliminary results[5] from this analysis are presented in Table 2. Other measurements of lepton asymmetry parameters are also listed for completeness. The uncertainties in all these different measurements are dominated by statistics. If lepton universality is assumed, the measurements may be combined to yield

$$A_l = 0.1542 \pm 0.0037, \tag{15}$$

$$\sin^2 \theta_W^{eff} = 0.23061 \pm 0.00047. \tag{16}$$

This value of $\sin^2 \theta_W^{eff}$ can be compared with the LEP average[8] of 0.23157 ± 0.00042, obtained from lepton forward-backward asymmetries and τ polarization measure-

ments. The SLD and LEP lepton averages agree within 1.5 σ.

1.4 Heavy Quark Asymmetries

Measurements of the heavy quark asymmetry parameters A_b and A_c provide complementary information to that obtained from the precise left-right asymmetry measurement. As pointed out earlier, A_b and A_c are particularly sensitive to vertex corrections. Extraction of pure samples of heavy quark events is greatly aided by two unique features of the SLC/SLD. First, the transverse dimensions of the SLC luminous region is of order of 1 μm^2 and the interaction point is very stable over time. Second, SLD is equipped with a high-resolution pixel CCD Vertex Detector[9] (VXD) which provides true three-dimensional information and a single hit resolution of 5.6 μm in the $r\phi$ plane (transverse to the beam axis) and 6.2 μm in the rz plane (containing the beam axis). The inner VXD radius is 2.95 cm and there is a minimum of two hits per track within $|\cos\theta| < 0.74$ — the average number of hits is 2.3. Tracking is performed by combining information from the CDC[10] with that from the VXD. The combined impact parameter resolution at high momentum is determined from $Z^0 \to \mu^+\mu^-$ decays to be $\sigma(r\phi) = 11$ μm and $\sigma(rz) = 37$ μm. Multiple scattering yields an additional momentum-dependent contribution parameterized as $\sigma = 70$ μm$/(p \, \sin^{3/2}\theta)$, where the momentum p is expressed in GeV/c. The transverse position of the IP is determined using samples of ~ 30 consecutive hadronic Z^0 decays with an accuracy of 7 ± 2 μm. The longitudinal IP position is determined on an event-by-event basis with an accuracy of 32 μm for Z^0 decays into light-flavor quarks (uds), 36 μm for $Z^0 \to c\bar{c}$ decays, and 52 μm for $Z^0 \to b\bar{b}$ decays, as determined from the Monte Carlo (MC). Detailed description of the procedures and performance of the tracking system may be found elsewhere.[11]

Another (almost) unique feature of the SLD is the Cherenkov Ring Imaging Detector[12] (CRID) which allows charged particle identification over most of the momentum range. The CRID contains both a liquid radiator and a gas radiator system (see Fig. 3). The liquid radiator provides low momentum identification with π/K (K/p) separation up to ~ 4 GeV/c (~ 8 GeV/c), whereas the gas radiator provides π/K (K/p) separation above ~ 2.5 GeV/c (~ 9 GeV/c).

Three different techniques have been used to measure the b-quark asymmetry parameter A_b. These differ mostly by the method used to determine which hemi-
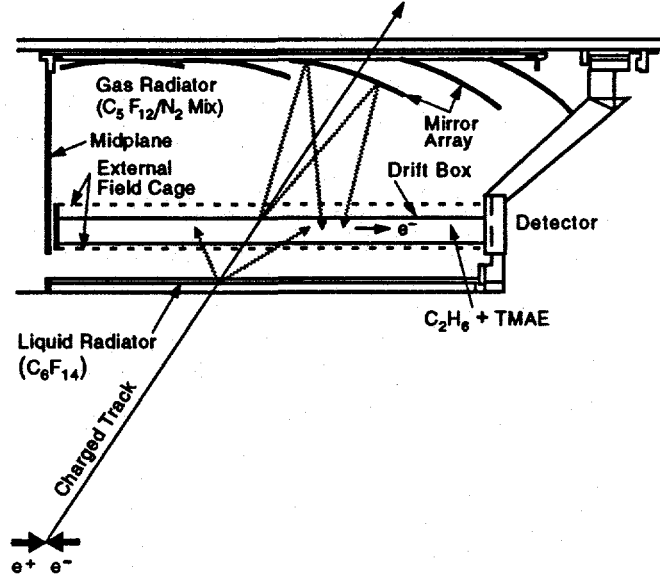
8

Figure 3: Cross-section view of one CRID quadrant.

sphere contains the primary b-quark: jet charge, kaon charge, or lepton charge. The first step (after hadronic event selection) in each analysis is to tag $Z^0 \to b\bar{b}$ events either by requiring that the number of tracks with two-dimensional impact parameter greater than $3\,\sigma$ be greater or equal to three, or by utilizing the fact that leptons from B hadron decays have harder p and p_T (with respect to the jet axis) distributions than from other processes.

A_b is determined with a fit to the $\cos\theta$-dependent differential cross-section [Eq. (4)] with the electron beam polarization as input. The thrust axis direction is used to provide the primary quark axis, except for the lepton analysis which uses the jet axis.

1.4.1 A_b with Jet Charge

The first step of the analysis is the selection of $Z^0 \to b\bar{b}$ events by requiring the event to contain at least three tracks with signed normalized $r\phi$ impact parameter $\delta/\sigma_\delta > 3$. This yields a sample with a $b\bar{b}$ purity of 89% and an efficiency of 61%. The $b/\bar{b}$ tag is provided by a momentum-weighted track charge defined as

$$Q_{\text{diff}} = Q_b - Q_{\bar{b}} = -\sum Q_{\text{track}} \left| \vec{p} \cdot \hat{T} \right|^\kappa \text{sign}\left(\vec{p} \cdot \hat{T} \right), \qquad (17)$$

where $\vec{p}$ is the three-momentum of each track and Q_{track} its charge, $\hat{T}$ is the direction of the event thrust axis, signed such as to make $Q_{\text{diff}} > 0$, and the

9

coefficient $\kappa = 0.5$ is chosen to maximize the analyzing power of the tag. The quantity Q_{diff} represents the difference between the momentum-weighted charges in the two event hemispheres — separated by the plane perpendicular to the thrust axis. $\hat{T}$ is thus an estimate of the b-quark direction. This tag is commonly referred to as "jet charge". A quantity related to Q_{diff} is the sum of the momentum-weighted charges in the two hemispheres defined as

$$Q_{\text{sum}} = Q_b + Q_{\bar{b}} = \sum Q_{\text{track}} \left| \vec{p} \cdot \hat{T} \right|^{\kappa}. \tag{18}$$

Due to its high efficiency ($\sim$ 100%), the jet charge tag lends itself to self-calibration, i.e., the analyzing power of the $b/\bar{b}$ tag can be determined directly from the data which reduces the systematic sensitivity to $Z^0 \to b\bar{b}$ modeling in the MC. The self-calibration is performed by comparing the momentum-weighted charges in the two hemispheres or more specifically by comparing the widths of the $|Q_{\text{diff}}|$ and $|Q_{\text{sum}}|$ distributions. If we make the (excellent) assumption that the momentum-weighted charge obeys a Gaussian distribution, the probability to correctly tag the primary $b/\bar{b}$ quark becomes

$$P_{\text{correct}} = \frac{1}{1 + e^{-\alpha_b |Q_{\text{diff}}|}}, \tag{19}$$

where the constant α_b is defined in terms of the widths σ_{diff} and σ_{sum} as determined from the distributions of $|Q_{\text{diff}}|$ and $|Q_{\text{sum}}|$ observed in the data

$$\alpha_b = \frac{2\sqrt{2 \left(\frac{\sigma_{\text{diff}}}{\sigma_{\text{sum}}} - 1 \right)}}{\sigma_{\text{sum}}}, \tag{20}$$

$$= 0.253 \pm 0.013 \quad \text{for 1993-95 data.} \tag{21}$$

The average correct tag probability is thus $\langle P_{\text{correct}} \rangle = 68\%$. The expression for α_b is modified slightly to take into account correlations between the two hemispheres. The correlation is estimated to be 2.9% by the Monte Carlo simulation. It arises mostly from the correlation between the total charges of the two hemispheres imposed by charge conservation in the event as a whole.

The forward-backward asymmetries obtained for left- and right-handed electron beams are shown in Fig. 4. The magnitude of the asymmetry is clearly more pronounced for the 1994-95 data than for the 1993 data, as expected from the increase in beam polarization for the 1994-95 data. A likelihood analysis using a $|Q_{\text{diff}}|$-dependent analyzing power derived from Eq. (19) and including a
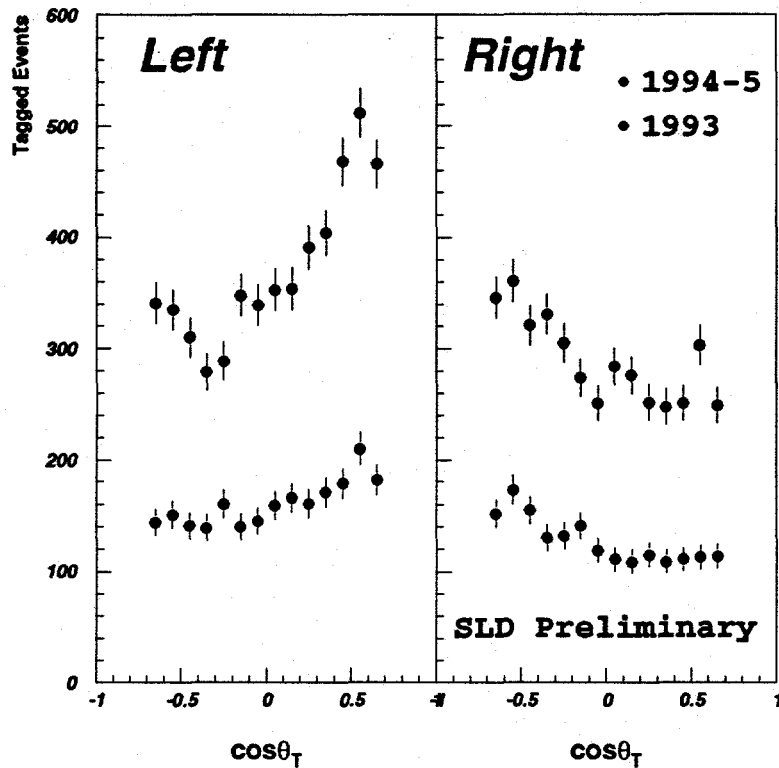
Figure 4: Distributions of the thrust axis $\cos\theta$ for left- and right-handed electron beams. The lower (upper) set of points correspond to 1993 (1994–95) data.

$\cos\theta$-dependent QCD correction yields

$$A_b = 0.843 \pm 0.046(\text{stat}) \pm 0.051(\text{syst}). \tag{22}$$

The main contributions to the systematic error are: (i) $\delta A_b/A_b = 3.7\%$ from uncertainties in the magnitude of the hemisphere correlation, as determined by comparing different fragmentation models (JETSET 7.4 and HERWIG 5.7); (ii) $\delta A_b/A_b = 3.0\%$ from the statistical uncertainty in determining the value of α_b from the 1993–95 data; (iii) $\delta A_b/A_b = 2.6\%$ from the uncertainties in the event sample composition after the $b\bar{b}$ event tag (mostly uncertainty in R_c).

1.4.2 A_b with Kaons

This analysis proceeds with the same $b\bar{b}$ event tag as the Jet Charge analysis but differs in the technique used to perform the $b/\bar{b}$ tag. Here the tag exploits

11

the dominant $b \to c \to s$ transition in B decays. Therefore, detection of K^- (K^+) mesons tags b ($\bar{b}$) quarks. Right-sign kaon production has been measured by ARGUS[13] in B^+ and B_d^0 decays to be $(85 \pm 5)\%$ and $(82 \pm 5)\%$ respectively. Some dilution is expected due to $b \to c\bar{c}s$ transitions and $s\bar{s}$ production in B or D decays. The analysis presented here is the first application of kaon tagging for a heavy quark asymmetry measurement.

Charged kaon track candidates are required to have signed $r\phi$ normalized impact parameter $\delta/\sigma_\delta > 1.5$ and $3 < p < 20$ GeV/c. These cuts select B decay products preferentially. Kaons are identified with the CRID (gas radiator only). The main uncertainty in the identification comes from knowledge of the rate of charged pions misidentified as kaons. An overall $\pi \to K$ misidentification rate of 7.2% is measured using pure samples of pions from one-prong and three-prong τ decays for which the true $K^\pm$ component is well-measured and small. The cuts yield a sample with 75% kaon purity.

Figure 5 shows the distribution of the cosine of the angle between the thrust axis and the electron beam directions signed by the tagging variable Q_K. This quantity is obtained by computing the difference between the sum of kaon charges in each hemisphere: $Q_K = \sum_i^{Hemi1} Q_i - \sum_j^{Hemi2} Q_j$, where Q_i is the charge of kaon track i. As a result, 30% of the selected events are tagged with a correct $b/\bar{b}$ tag probability estimated to be 71% from the Monte Carlo simulation. A clear forward-backward asymmetry is observed in Fig. 5 (the analysis was only applied to the 1994–95 data). The non-$b\bar{b}$ background is dominated by $c\bar{c}$ events and displays a similar asymmetry to the signal asymmetry. The $b/\bar{b}$ tag analyzing power in the MC is cross-checked in events with a kaon tag in each hemisphere. The fraction with opposite kaon charges is found to be $62.4 \pm 2.9\%$ in the data, in excellent agreement with a fraction of $61.9 \pm 1.5\%$ in the MC.

The measurement of A_b is derived by comparing data and Monte Carlo distributions of the left-right forward-backward asymmetry, as shown in Fig. 6. A binned fit to this distribution yields

$$A_b = 0.91 \pm 0.09(\text{stat}) \pm 0.09(\text{syst}). \qquad (23)$$

The systematic error is dominated by detector uncertainties ($\delta A_b/A_b = 6.2\%$ — mostly due to the uncertainty in the $\pi \to K$ misidentification rate) and by uncertainties in the modeling of B and D production and decay ($\delta A_b/A_b = 7.2\%$).
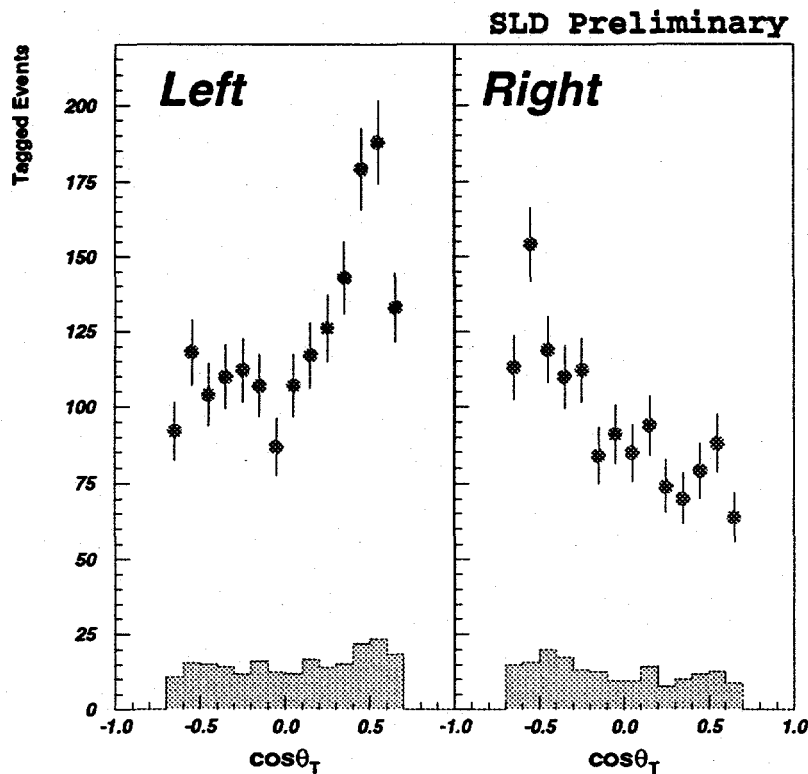
Figure 5: Distribution of the thrust axis $\cos\theta$ for left- and right-handed electron beams. The shaded portions indicate the contributions from non-$b\bar{b}$ events.

1.4.3 A_b and A_c with Leptons

Another approach to $b\bar{b}$ event selection and $b/\bar{b}$ tagging is to use leptons from semileptonic decays. The distinctive lepton total and transverse momenta are exploited as well as the charge of the lepton. In this analysis,[14] a measurement of the c-quark asymmetry parameter A_c is also extracted.

Electrons are identified using information from both the CDC and the LAC[15]: track momentum and pointing and energy deposition in the calorimeter. This information is incorporated into a neural network algorithm trained on Monte Carlo electrons. Furthermore, information from the CRID is also added which greatly improves the electron identification purity at low momentum. The identification efficiency is $\sim 55\%$ with a misidentification rate of less than 2% per charged pion.

Muons are identified using data from the tracking and Warm Iron Calorimeter[16] systems. As for the electron identification, CRID information is added to
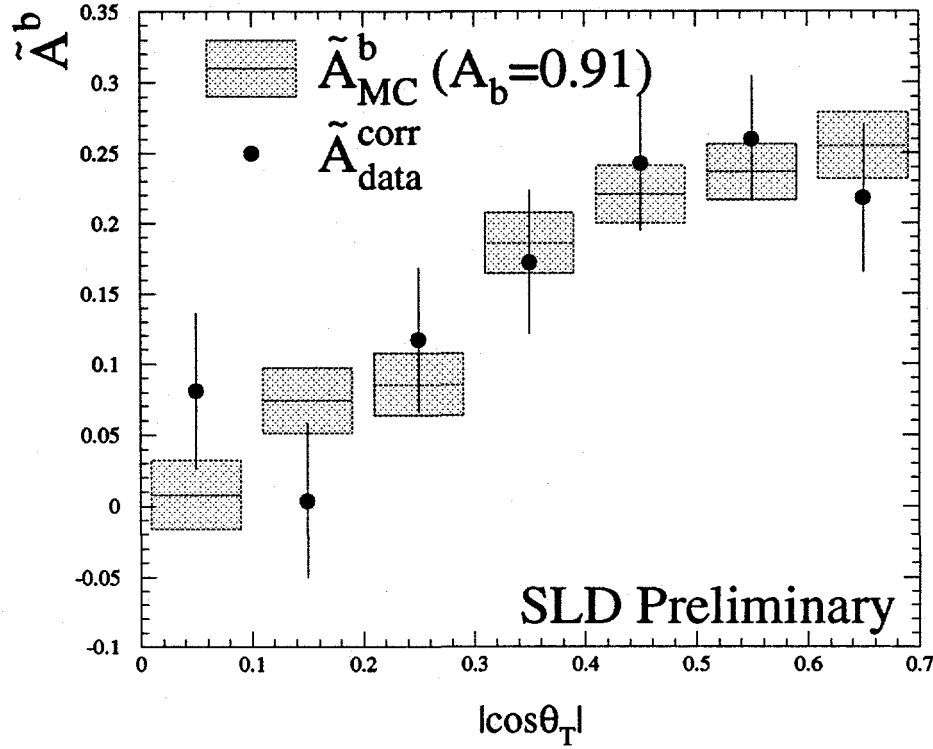
13

Figure 6: Distribution of the left-right forward-backward asymmetry as a function of the thrust axis $|\cos\theta|$ for data (points) and best fit MC (horizontal bands).

reject π, K, and p background. The efficiency is $\sim 80\%$ with a charged pion misidentification rate of less than 0.3%.

As for the jet charge analysis, the asymmetry parameters A_b and A_c are extracted with an unbinned likelihood analysis using the full differential cross-section [Eq. (4)] and which incorporates the sample components ($b \rightarrow l$, $b \rightarrow c \rightarrow l$, $c \rightarrow l$, etc.) as a function of lepton p and p_T as determined from the MC. The results for the 1994–95 data are:

$$\text{Muons} \quad A_b = \quad 0.874 \pm 0.107(\text{stat}) \pm 0.044(\text{syst}), \quad (24)$$

$$A_c = \quad 0.633 \pm 0.151(\text{stat}) \pm 0.072(\text{syst}), \quad (25)$$

$$\text{Electrons} \quad A_b = \quad 0.880 \pm 0.107(\text{stat}) \pm 0.051(\text{syst}), \quad (26)$$

$$A_c = \quad 0.620 \pm 0.162(\text{stat}) \pm 0.089(\text{syst}). \quad (27)$$

These measurements can be combined with our previously published results[17]

14

	$\delta A_b(\mu)$	$\delta A_b(e)$	$\delta A_c(\mu)$	$\delta A_c(e)$
MC statistics	0.022	0.026	0.012	0.035
Jet axis smearing	0.015	0.034	0.003	0.033
Detector simulation	0.022	0.011	0.034	0.045
Physics modeling	0.027	0.026	0.062	0.060
Total	0.044	0.051	0.072	0.089

Table 3: Systematic uncertainties in A_b and A_c measurements with lepton tags.

based on the 1993 data to yield

$$A_b = 0.882 \pm 0.068(\text{stat}) \pm 0.047(\text{syst}), \tag{28}$$

$$A_c = 0.612 \pm 0.102(\text{stat}) \pm 0.076(\text{syst}). \tag{29}$$

Systematic uncertainties are summarized in Table 3.

1.5 Combined A_b, A_c, and $Z^0 \to b\bar{b}$ Coupling

The above three A_b analyses have been combined taking into account correlated systematic uncertainties to yield an SLD average of $A_b(\text{SLD}) = 0.863 \pm 0.049$. This value is to be compared with the LEP average unpolarized forward-backward asymmetry for b quarks of $A_b^{FB\ 0}(\text{LEP}) = 0.0979 \pm 0.0028$.[8] Since the unpolarized asymmetry does not measure A_b directly, one has to use the world average value of $A_e = 0.1500 \pm 0.0025$ from the left-right asymmetry measurement at SLD and the lepton forward-backward asymmetry measurements at LEP.[8] The LEP measurement can then be translated into $A_b(\text{LEP}) = \frac{4}{3}\frac{A_b^{FB}}{A_e} = 0.870 \pm 0.025$. A combined SLD and LEP average value of $A_b = 0.869 \pm 0.022$ is obtained which is about three standard deviations away from the Standard Model prediction of 0.935.

Similarly, the lepton A_c measurement can be combined with a previous measurement[18] based on semi exclusive reconstruction of D^{*+} and D^+ mesons to yield an SLD average of $A_c(\text{SLD}) = 0.625 \pm 0.084$. This average is in good agreement with both the Standard Model ($A_c = 0.666$) and the LEP average derived from the c-quark forward-backward asymmetry measurements as above.

It is instructive to summarize our knowledge of the $Zb\bar{b}$ coupling in the context of the analysis proposed by Takeuchi, Grant, and Rosner.[19] Deviations from the
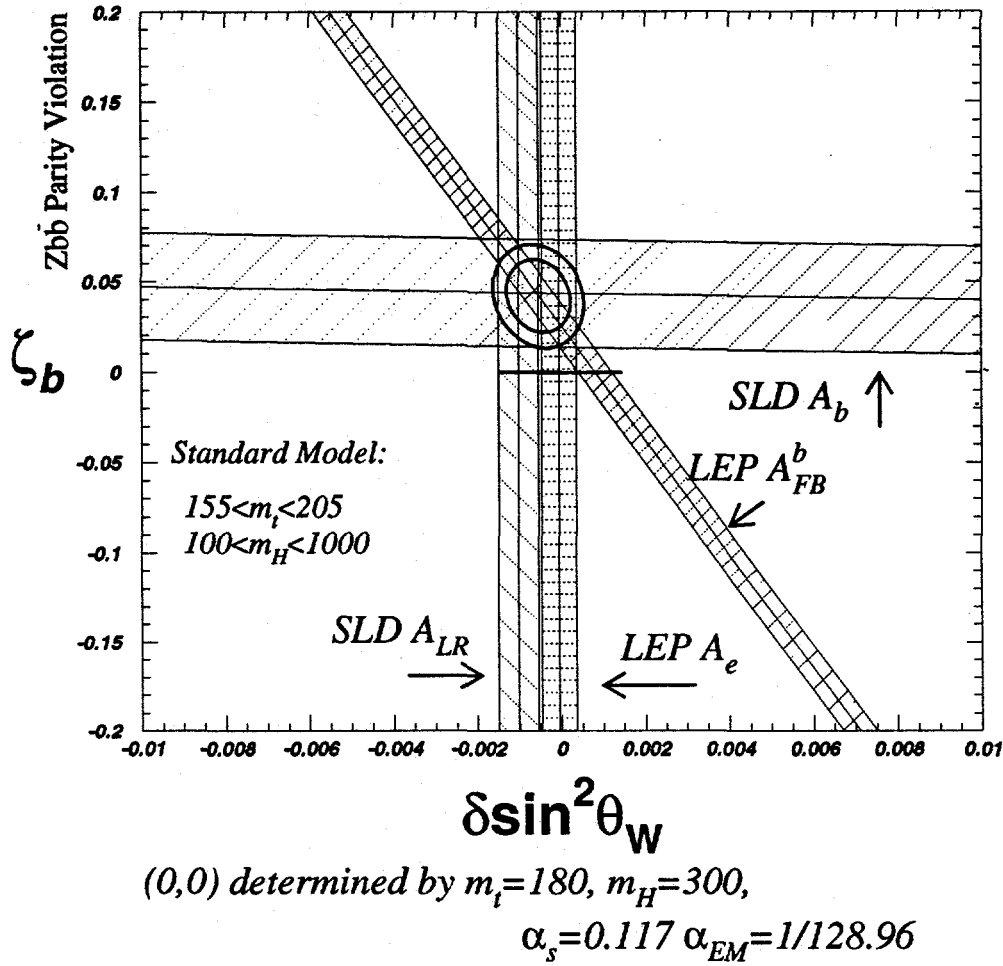
15

Figure 7: Deviation in the $Z^0 \rightarrow b\bar{b}$ coupling parity violation vs. the deviation in $\sin^2 \theta_W^{eff}$ for the Standard Model and all electroweak data.

Standard Model are parameterized in terms of radiative corrections $\delta \sin^2 \theta_W$, ξ_b, and ζ_b. The parameter ζ_b represents deviations in the parity violation of the $Zb\bar{b}$ coupling. As shown in Fig. 7, the A_{LR} and direct A_b asymmetry measurements are complementary, indicating the need for precise measurements of both quantities. The unpolarized forward-backward asymmetry A_b^{FB} measured at LEP cannot alone separate between deviations in $\sin^2 \theta_W^{eff}$ and $Z^0 \rightarrow b\bar{b}$ parity violation. The Standard Model for $155 < m_t < 205$ GeV/c^2 and $100 < m_H < 1000$ GeV/c^2 is represented by the thin horizontal band passing through the origin ($m_t = 180$ GeV/c^2, $m_H = 300$ GeV/c^2, $\alpha_s = 0.117$, and $\alpha_{em} = 1/128.96$) in the ζ_b vs. $\delta \sin^2 \theta_W^{eff}$ plane. The best fit to all electroweak data is indicated by the 68% and

16

90% C.L. contours. This fit displays the discrepancy between A_b measurements and the SM prediction.

1.6 Partial Width R_b

Another observable providing strong constraints on the Standard Model is the partial width of the Z^0 into $b\bar{b}$ final states $R_b = \Gamma(Z^0 \to b\bar{b})/\Gamma(Z^0 \to \text{hadrons})$. The measurement proceeds by first selecting a pure sample of $Z^0 \to$ hadrons events. Then each event hemisphere is b-tagged independently for the presence of a B hadron decay. By computing both the rate for tagging a hemisphere (F_s) and the rate for tagging both hemispheres in an event (F_d), one can extract both the value of R_b and the efficiency ϵ_b of the hemisphere tag. These are obtained by solving the following set of equations:

$$F_s = \epsilon_b R_b + \epsilon_c R_c + \epsilon_{uds}(1 - R_b - R_c), \tag{30}$$

$$F_d = \epsilon_b^{dbl} R_b + \epsilon_c^{dbl} R_c + \epsilon_{uds}^{dbl}(1 - R_b - R_c). \tag{31}$$

The Monte Carlo is used to estimate the charm and uds efficiencies for tagging hemispheres ϵ_c and ϵ_{uds}, and for tagging both hemispheres ϵ_c^{dbl} and ϵ_{uds}^{dbl}, so it is very important to increase the purity of the b-tag to reduce the potentially large systematic uncertainties mainly due to modeling of the charm production and decay. Correlations between hemispheres imply that the efficiency to tag both hemispheres is not simply ϵ_b^2 but rather $\epsilon_b^{dbl} = \epsilon_b^2 + \lambda_b(\epsilon_b - \epsilon_b^2)$, where λ_b is the correlation parameter to be determined from the MC.

SLD has designed a new approach to achieve high-efficiency and high-purity b-tagging. The excellent 3-D vertexing capabilities of the vertex detector allow B decays to be reconstructed with an inclusive topological technique.[20] Well-measured tracks are parameterized as Gaussian probability tubes in 3-D space [see Fig. 8(a)]. Using these a search is made to find regions in 3-D space with high "tube overlap" [see Fig. 8(b)]. The significance of the overlap is related to the number of tracks and their extrapolation errors, i.e., the track density. Such an overlap region, or "seed" vertex, is found in $\sim$ 50% of b hemispheres, but only in $\sim$ 15% of c hemispheres and in less than 1% of uds hemispheres. The b hemisphere vertex finding efficiency increases with the decay length D to attain a constant level of 80% for $D > 3$ mm. Due to the typical $B \to D$ cascade structure of the decays, not all tracks originate from a single space point, and
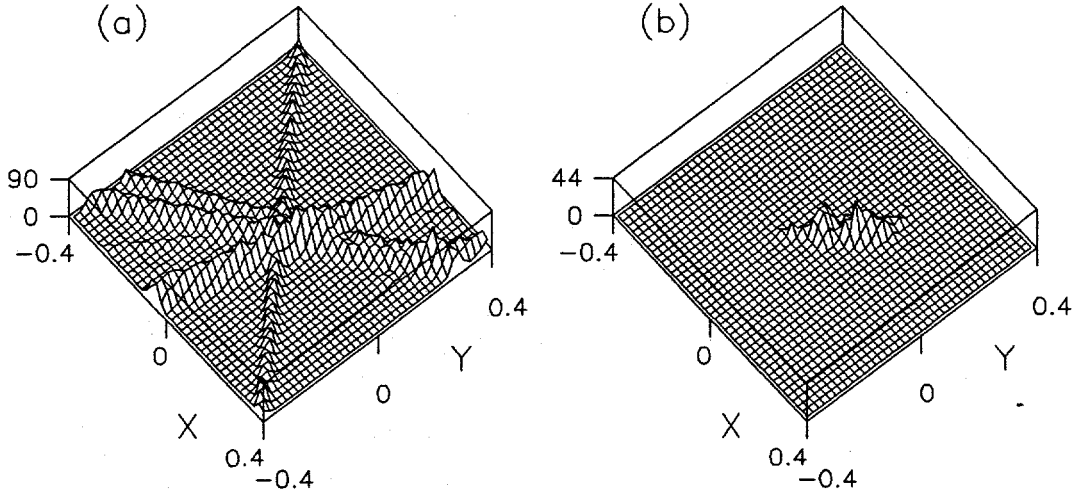
Figure 8: Two-dimensional projection of (a) tracks parameterized as Gaussian tubes and (b) regions of significant track overlap showing primary and secondary vertices.

thus, may not be attached to the seed vertex if the D meson travelled sufficiently far from the B decay point. Therefore, an attempt is made to attach isolated tracks to the seed vertex to form the final secondary vertex. Requirements for attachment are: $T < 1$ mm, $L/D > 0.25$, and $L > 1$ mm, where the quantity T represents the minimum distance between a given track and the seed vertex axis, and L is the distance along the vertex axis between the interaction point and the point of closest approach between the track and the vertex axis (see Fig. 9).

The variable used to tag b hemispheres is the mass of the reconstructed vertex. First, the invariant mass M_{raw} of all charged tracks associated with the secondary vertex is computed (tracks are assumed to be pions). A clear separation between b hemispheres and the rest can be observed in Fig. 10(a). In particular, the charm contribution vanishes above the natural cutoff mass of ~ 2 GeV/c^2. Improved efficiency for b hemisphere tagging can be obtained by exploiting kinematical information. This is achieved by constructing the p_T-added mass

$$ M = \sqrt{M_{raw}^2 + p_T^2} + |p_T|, \tag{32} $$

where p_T is the total momentum of all tracks in the vertex in the plane perpendicular to the vertex axis. The value of p_T is chosen to be the smallest one allowed by the uncertainties in the vertex and IP positions (which affect the direction of the vertex axis). This and the requirement that $M \leq 2 M_{raw}$ reduces the contam-
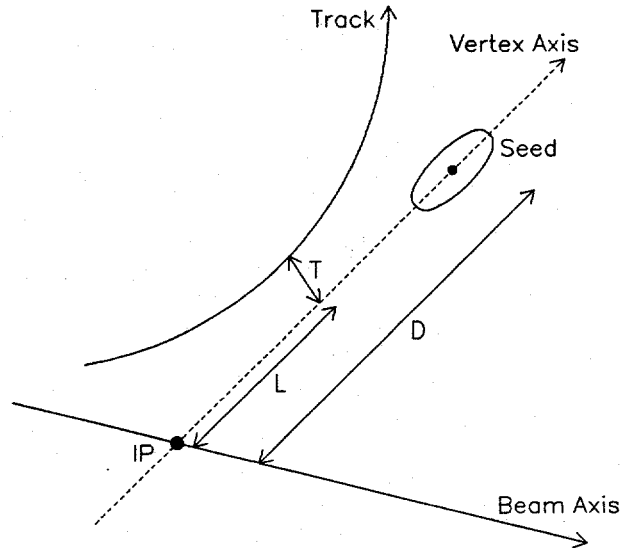
18

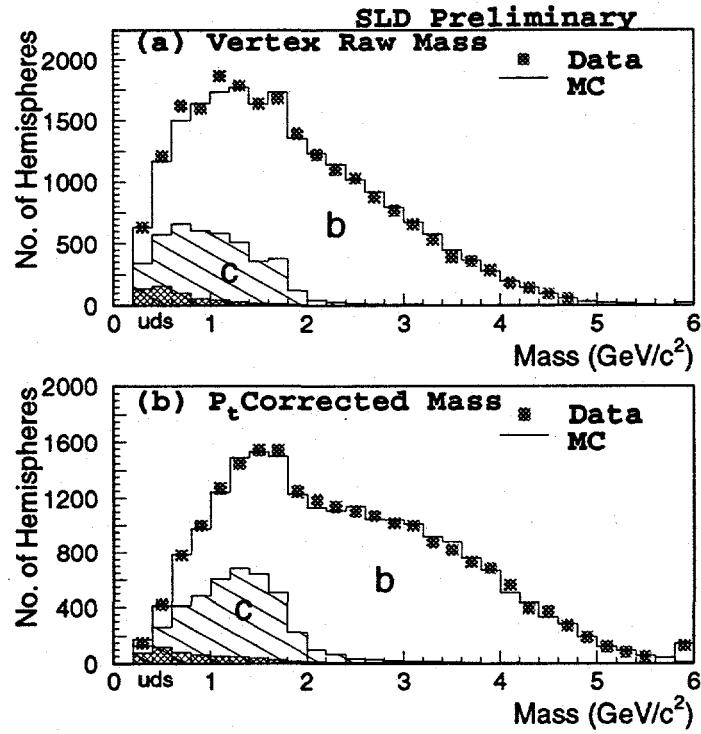Figure 9: Definition of track variables used to attach isolated tracks to secondary vertices.

Figure 10: Distributions of (a) raw mass and (b) p_T-added mass for topological vertices.

ination from non-b hemispheres in the high-mass region. As a result, the b-tag efficiency is enhanced by approximately 40% without significant degradation in purity [see Fig. 10(b)].

For the final analysis, vertices are required to satisfy $D > 1$ mm and $M > 2$ GeV/c^2. The corresponding b-tag purity and the correlation between b hemispheres are estimated from the Monte Carlo to be 97.3% and $\lambda_b = 0.33\%$, respectively. Solving Eqs. (30) and (31) yields

$$R_b = 0.2149 \pm 0.0033(\text{stat}) \pm 0.0021(\text{syst}) \pm 0.0007(R_c),$$

$$\epsilon_b = 36.8 \pm 0.6\%.$$

The value of the mass cut was chosen to minimize the overall uncertainty on R_b as shown in Fig. 11 but is currently dominated by the statistical uncertainty.
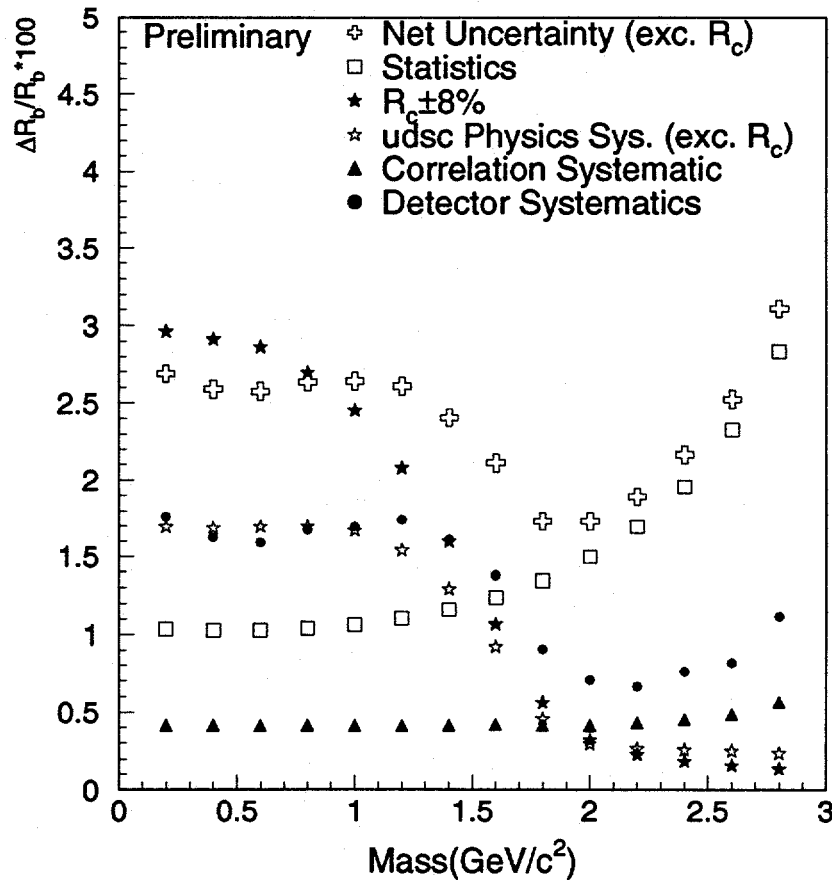

Figure 11: R_b uncertainty components as a function of mass cut.

The SLD and LEP measurements are compared in Fig. 12. Our measured value is consistent with both the LEP average and the SM prediction.
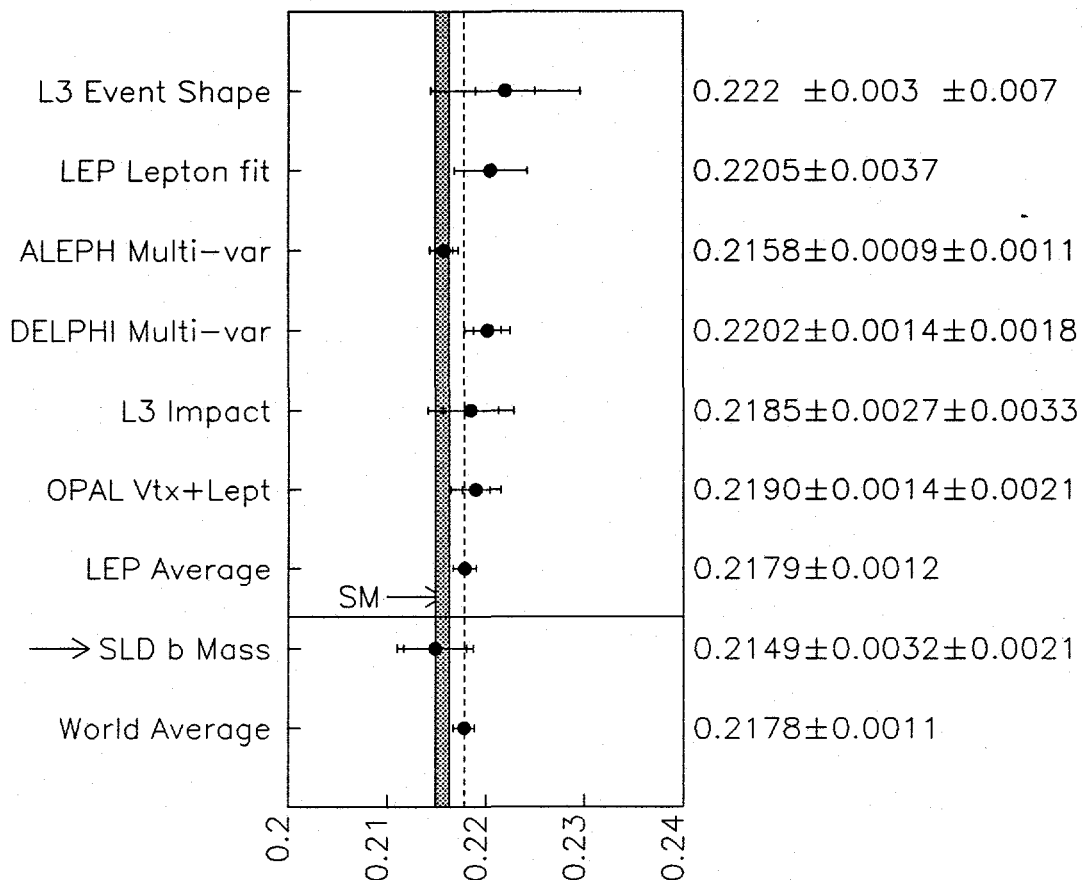

L3 Event Shape		0.222 ±0.003 ±0.007
LEP Lepton fit		0.2205±0.0037
ALEPH Multi−var		0.2158±0.0009±0.0011
DELPHI Multi−var		0.2202±0.0014±0.0018
L3 Impact		0.2185±0.0027±0.0033
OPAL Vtx+Lept		0.2190±0.0014±0.0021
LEP Average		0.2179±0.0012
SLD b Mass		0.2149±0.0032±0.0021
World Average		0.2178±0.0011

Figure 12: R_b measurements from LEP and SLD.

2 B Physics

Several aspects of the weak interaction can be probed by studying the weak decays of B hadrons. First, by measuring lifetimes, we can test our understanding of B hadron decay dynamics. Second, we can test the Cabibbo-Kobayashi-Maskawa (CKM) quark mixing matrix description within the Standard Model. In particular, this helps constrain CP violation predictions. Measurements of the lifetimes of B^+ and B_d^0 mesons, and of the time dependence of B_d^0–$\overline{B_d^0}$ mixing, are presented below.

2.1 B^+ and B_d^0 Lifetimes

As explained above, measurements of the B hadron lifetimes are important to test our understanding of B hadron decay dynamics. In the naive spectator model, all hadrons containing one heavy quark Q are predicted to have the same lifetime. Specifically, one expects $\tau(B^+) = \tau(B_s^0) = \tau(B_d^0) = \tau(\Lambda_b)$. However, a strong hierarchy is observed in the case of charm hadrons: $\tau(D^+) \simeq 2.3\, \tau(D_s) \simeq 2.5\, \tau(D^0) \simeq 5\, \tau(\Lambda_c^+)$. This hierarchy is predicted[21] to scale with $1/m_Q^2$ and is thus expected to yield much smaller lifetime differences for B hadrons. In the case of B^+ and B_d^0, a calculation[21] based on an expansion in terms of $1/m_Q$ predicts $\tau(B^+)/\tau(B_d^0) = 1 + 0.05(f_B/200\mathrm{MeV})^2$, where f_B is the B hadron decay constant. Lifetimes for different B hadrons are thus predicted to be less than 10%. Exclusive and inclusive B lifetimes are also important because they are necessary inputs to many other measurements, as for example, many electroweak $Z^0 \to b\bar{b}$ measurements, time-dependent B_d^0–$\overline{B_d^0}$ mixing measurements, and precise determinations of the CKM matrix element $|V_{cb}|$.

Several techniques have been used to measure the B^+ and B_d^0 lifetimes. The cleanest method reconstructs samples of B^+ and B_d^0 decays exclusively. However, the branching fractions for such exclusive reconstruction are typically small ($\sim 10^{-4} - 10^{-3}$). Most measurements have relied on samples of semileptonic B decays where the $D^{(*)}$ meson is exclusively reconstructed and intersected with an identified lepton to determine the B decay point. The lifetime measurements then rely on assumptions concerning the B^+ and B_d^0 content of the selected $\overline{D^0}Xl^+\nu$ and $D^{(*)-}Xl^+\nu$ samples.

The two techniques used by SLD take advantage of the excellent 3-D vertexing capabilities of the VXD to reconstruct the decays (semi-) inclusively. The goal is to reconstruct and identify all the tracks originating from the B decay chain. This then allows charged and neutral B mesons to be separated by simply measuring the total charge of tracks associated with the B decay.

The first analysis[22] uses the inclusive topological vertexing technique described earlier (see Sec. 1.6) but the criteria used to attach tracks to seed vertices are slightly different: $T < 1$ mm, $L/D > 0.3$, and no minimum cut on L. In the hadronic Z^0 event sample, we select 9719 B decay candidates by requiring $M_{raw} > 2$ GeV/c^2 and $D > 1$ mm. The minimum vertex mass requirement serves not only as a means to select a 97% pure sample of $b\bar{b}$ events but also as a means to enhance

the charge reconstruction purity. The sample is divided into neutral and charged subsamples corresponding to reconstructed decays with total charge $Q = 0$ or $Q = \pm 1, 2, 3$, respectively, where Q is the charge sum of all tracks associated with the vertex. The charged (neutral) sample consists of 6033 (3665) decays. Monte Carlo studies show that the charged (neutral) sample is 97.3% (98.0%) pure in B hadrons. The simulated flavor contents are 54.6% B^+, 30.5% B_d^0, 8.6% B_s^0, and 3.6% B baryons for the charged sample, and 23.3% B^+, 54.5% B_d^0, 14.6% B_s^0, and 5.6% B baryons for the neutral sample*. The sensitivity of this analysis to the individual B^+ and B_d^0 lifetimes can be assessed from the 1.8 (2.3) ratio of $B^\pm (B_d^0)$ decays over $B_d^0 (B^+)$ decays in the charged (neutral) sample.

The B^+ and B_d^0 lifetimes are extracted with a simultaneous binned maximum likelihood fit to the decay length distributions of the charged and neutral samples (see Fig. 13). These distributions are compared with MC distributions obtained
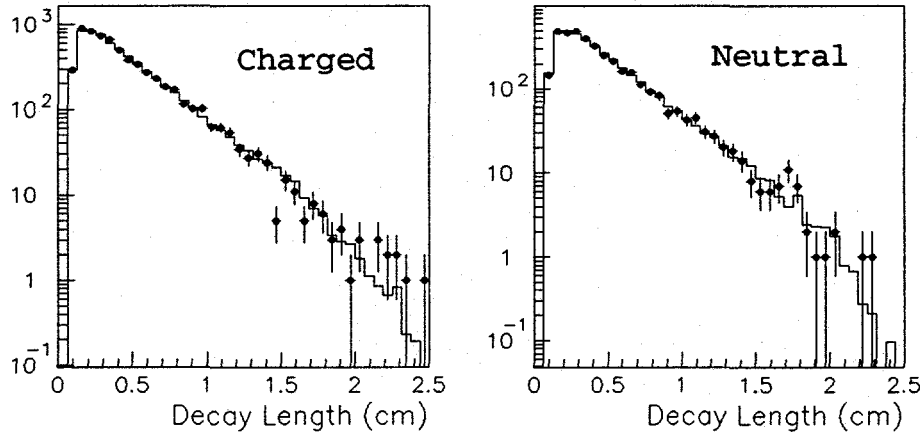

Figure 13: Decay length distributions for data (points) and best fit Monte Carlo (histogram) in the topological analysis.

for a range of values of the B^+ and B_d^0 lifetimes. The maximum likelihood fit yields lifetimes of

$$\tau_{B^+} = 1.69 \pm 0.06(\text{stat}) \pm 0.06(\text{syst}) \text{ ps}, \tag{33}$$

$$\tau_{B_d^0} = 1.63 \pm 0.07(\text{stat}) \pm 0.08(\text{syst}) \text{ ps}, \tag{34}$$

---

*Reference to a specific state (e.g., B^+) implicitly includes its charge conjugate state (i.e., B^-).

with a lifetime ratio of

$$\frac{\tau_{B^+}}{\tau_{B_d^0}} = 1.04^{+0.08}_{-0.07}(\text{stat}) \pm 0.06(\text{syst}). \tag{35}$$

The main contributions to the systematic error come from uncertainties in the detector modeling, B_s^0 lifetime, fit systematics, and MC statistics.

The second lifetime analysis[23] is restricted to semileptonic decays which reduces the overall efficiency compared to the topological method but results in an improved charge reconstruction purity. In the semileptonic method, a D decay vertex is reconstructed topologically and the B decay vertex is formed by intersecting the D meson trajectory with that of an identified lepton. An attempt is then made to attach a slow-pion candidate to the B vertex to reconstruct the track topology of B decays into D^{*+} mesons.

The analysis selects identified electrons and muons with momentum transverse to the nearest jet axis > 0.4 GeV/c and results in a sample of 634 charged and 584 neutral decays. Monte Carlo studies show that the remaining charged (neutral) sample is 97.5% (99.1%) pure in B hadrons. The simulated flavor contents are 66.9% B^+, 22.5% B_d^0, 5.7% B_s^0, and 2.4% B baryons for the charged sample, and 19.6% B^+, 60.8% B_d^0, 14.0% B_s^0, and 4.7% B baryons for the neutral sample. The sensitivity of this analysis to the individual B^+ and B_d^0 lifetimes can be assessed from the 3:1 ratio of $B^+ (B_d^0)$ decays over $B_d^0 (B^+)$ decays in the charged (neutral) sample.

As for the topological analysis, the B^+ and B_d^0 lifetimes are extracted from the decay length distributions of the charged and neutral samples (see Fig. 14). The fit yields the following results:

$$\tau_{B^+} = 1.60^{+0.12}_{-0.11}(\text{stat}) \pm 0.06(\text{syst}) \text{ ps},$$

$$\tau_{B_d^0} = 1.55^{+0.13}_{-0.12}(\text{stat}) \pm 0.09(\text{syst}) \text{ ps},$$

with a ratio of

$$\frac{\tau_{B^+}}{\tau_{B_d^0}} = 1.03^{+0.15}_{-0.13}(\text{stat}) \pm 0.08(\text{syst}).$$

As in the case of the topological analysis, the dominant sources of systematic error are due to uncertainties in the detector modeling, B_s^0 lifetime, fit systematics, and MC statistics.

The two analyses described above yield lifetime measurements in agreement with those from other experiments (see Fig. 15) and with the expectation that the B^+ and B_d^0 lifetimes are nearly equal.
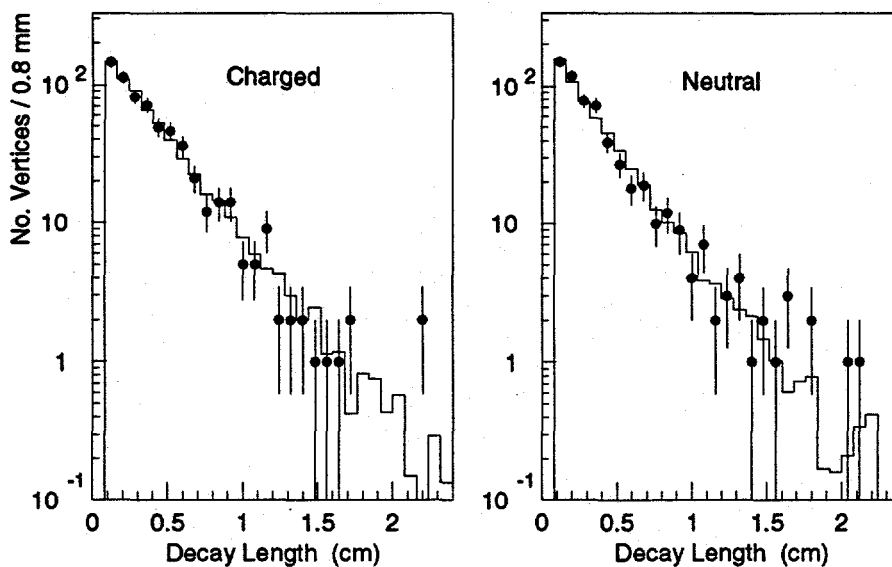
24

Figure 14: Decay length distributions for data (points) and best fit Monte Carlo (histogram) in the semileptonic analysis.
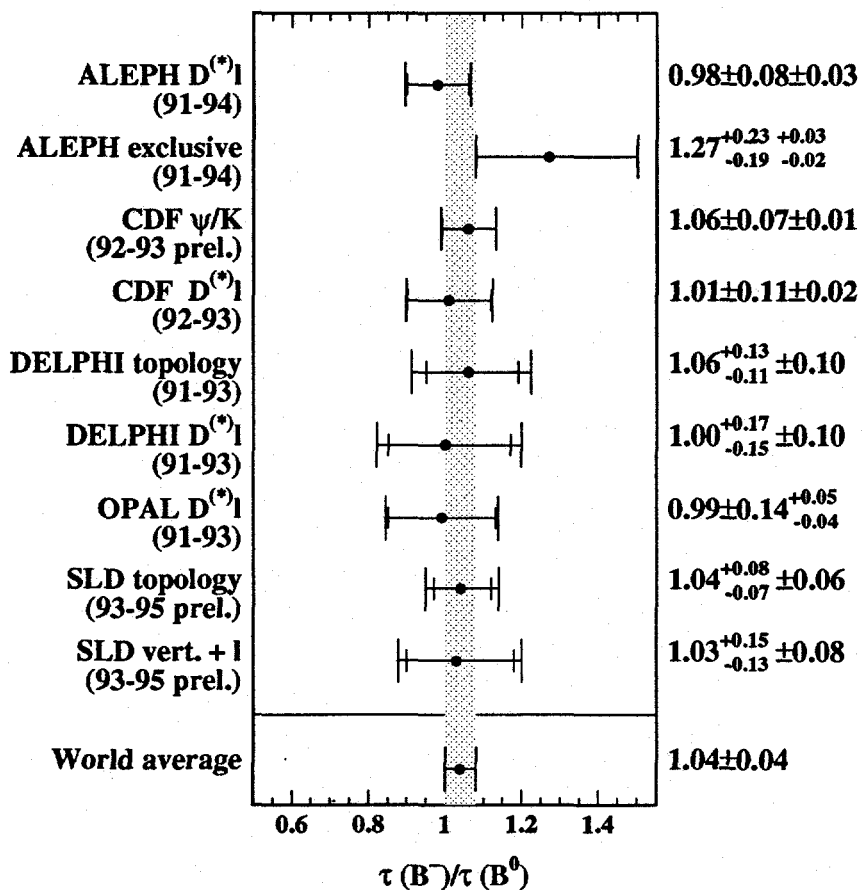

Figure 15: Comparison between measurements of the B^+/B^0_d lifetime ratio.

2.2 B^0–$\overline{B^0}$ Mixing

The phenomenon of B^0–$\overline{B^0}$ mixing is now well-established. Transitions between flavor states $B^0 \to \overline{B^0}$ take place via second order weak interactions "box diagrams". As in the case of the $K^0 - \overline{K^0}$ system, the weak eigenstates are linear combinations of the flavor eigenstates:

$$|B_L\rangle = \frac{1}{\sqrt{2}} \left(|B^0\rangle + |\overline{B^0}\rangle \right), \tag{36}$$

$$|B_H\rangle = \frac{1}{\sqrt{2}} \left(|B^0\rangle - |\overline{B^0}\rangle \right), \tag{37}$$

where $|B_L\rangle$ and $|B_H\rangle$ represent the light and heavy eigenstates (the effect of CP violation has been neglected). Due to the difference in mass between these eigenstates, they propagate differently in time, which gives rise to time-dependent oscillations between B^0 and $\overline{B^0}$ flavor eigenstates. Given an initial B^0 produced at $t = 0$, the probability that it decays as a B^0 at time t is given by

$$P_{B^0 \to B^0}(t) = \Gamma e^{-\Gamma t} \frac{1}{2} \left[1 + \cos(\Delta m t) \right], \tag{38}$$

whereas the probability that it decays as a $\overline{B^0}$ at time t is given by

$$P_{B^0 \to \overline{B^0}}(t) = \Gamma e^{-\Gamma t} \frac{1}{2} \left[1 - \cos(\Delta m t) \right], \tag{39}$$

where $\Gamma = 1/\tau$ is the B^0 decay width, Δm is the mass difference between the weak eigenstates and the lifetime difference between the weak eigenstates has been neglected since it is expected to be small. Thus, measuring the oscillation frequency of B^0–$\overline{B^0}$ mixing provides a measurement of Δm. The value of Δm can be calculated from the box diagrams for which the dominant contribution comes from virtual top quark exchange,

$$\Delta m_q = \frac{G_F^2}{6\pi^2} m_t^2 m_{B_q} F(m_t/m_W) \eta_{QCD} f_{B_q}^2 B_{B_q} \left| V_{tb}^* V_{tq} \right|, \tag{40}$$

where $q = d, s$ applies to either B_d^0 or B_s^0 mesons. Measuring Δm_q is thus sensitive to the CKM matrix element $|V_{tq}|$ for which little is known experimentally. There are large uncertainties in the theoretical estimates[24] of the term $f_{B_q}^2 B_{B_q}$ but these uncertainties are much reduced for the ratio between Δm_d and Δm_s. Thus, combining measurements of the oscillation frequency of both B_d^0–$\overline{B_d^0}$ and B_s^0–$\overline{B_s^0}$ mixing translates into a measurement of the ratio $|V_{td}|/|V_{ts}|$.

Experimentally, a measurement of the time dependence of B^0–$\overline{B^0}$ mixing requires three ingredients: (i) the B decay and its proper time have to be reconstructed, (ii) the B flavor at production (initial state $t = 0$) needs to be determined, as well as (iii) the B flavor at decay (final state $t = t_{decay}$). At SLD, the time dependence of B_d^0–$\overline{B_d^0}$ mixing has been measured using four different methods. All four use the same initial state tagging but differ by the method used to either reconstruct the B decay or tag its final state.

Initial state tagging takes advantage of the large polarization-dependent forward backward asymmetry in $Z^0 \to b\bar{b}$ decays

$$\tilde{A}_{FB}(\cos\theta_T) = 2A_b \frac{A_e - P_e}{1 - A_e P_e} \frac{\cos\theta_T}{1 + \cos^2\theta_T} \tag{41}$$

which is derived from Eq. (4). This only requires knowledge of the electron beam polarization P_e and the cosine of the angle between the thrust axis direction and the electron beam direction, $\cos\theta_T$. The tag works as follows. For left- (right-) handed electrons and forward (backward) B decay vertices, the initial quark is tagged as a b quark; otherwise, it is tagged as a $\bar{b}$ quark. The initial state tag can be augmented by using the momentum-weighted track charge (see Sec. 1.4.1) in the hemisphere opposite that of the reconstructed B vertex. Figure 16 shows the
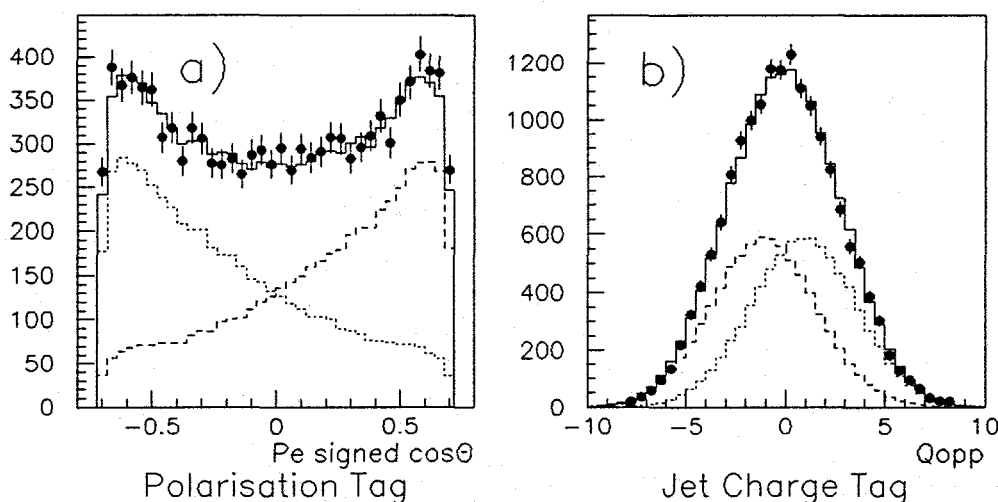

Figure 16: Distributions of (a) polarization-signed $\cos\theta_T$ and (b) opposite hemisphere jet charge for data (points) and MC (solid line). The MC b and $\bar{b}$ components are shown with dotted and dashed lines respectively.

distributions of $\cos\theta_T$ signed by the electron beam helicity and opposite hemi-

sphere jet charge. Clear separation between initial b and $\bar{b}$ quarks is observed. The polarized forward-backward asymmetry and the jet charge tags are combined to yield an initial state tag with 100% efficiency and effective average right-tag probability of 84% (for $\langle P_e \rangle = 77\%$).

The first two B_d^0–$\overline{B_d^0}$ mixing analyses[25] use topological vertexing (see Sec. 1.6) to select the tracks from the B decay and measure its decay length. A sample of 16803 vertices is selected after requiring $M > 2$ GeV/c^2 (no explicit cut is placed on the decay length). The first analysis uses charged kaons from the B decay chain to tag the final state. This tag relies on the fact that most B decays occur via the dominant $b \rightarrow c \rightarrow s$ transition and is similar to the tag used for the measurement of A_b presented in Sec. 1.4.2. Charged kaons are identified with the CRID, but for this analysis, both liquid and gas radiators are used to cover most of the kaon momentum range: 0.8 to 25 GeV/c. The tag variable here consists of the sum of identified kaon charges Q_K for charged tracks in the vertex such that $\sum Q_K > 0$ (< 0) tags B_d^0 ($\overline{B_d^0}$) decays. The rate of pion misidentification as a function of momentum is calibrated from the data using a pure sample of pions from K_s^0 decays. The kaon tag is available for 1/3 of the reconstructed decays and yields a sample of 5694 decays with a correct tag probability of 77% for B_d^0 decays.

Measurement of the time dependence of B_d^0–$\overline{B_d^0}$ mixing is extracted by computing the fraction of decays tagged as mixed as a function of decay length. It is not necessary to reconstruct the proper time because of the slow oscillation frequency of B_d^0–$\overline{B_d^0}$ mixing. A decay is tagged as mixed if the initial and final state tags disagree. A binned χ^2 fit is performed by comparing the distributions of the mixed fraction as a function of decay length obtained for the data and the MC for a range of Δm_d values. Figure 17(a) shows the mixed fraction distribution for the charged kaon analysis. A clear oscillation signal is observed. The fit yields a frequency of $\Delta m_d = 0.580 \pm 0.066(\text{stat}) \pm 0.075(\text{syst})$ ps^{-1} with a $\chi^2/\text{dof} = 10.2/10$. The main contributions to the systematic error arise from uncertainties in the $\pi \rightarrow K$ misidentification calibration from the data, in the rate of right-sign kaon production in B^+ and B_d^0 decays as measured by ARGUS,[13] and in the dependence of the fit results on binning and fit range, as summarized in Table 4.

The second analysis exploits the $B \rightarrow D$ cascade charge structure to tag the final state. To enhance the B_d^0 fraction in the sample of topological vertices, the total charge of tracks associated with the vertex is required to be equal to zero.
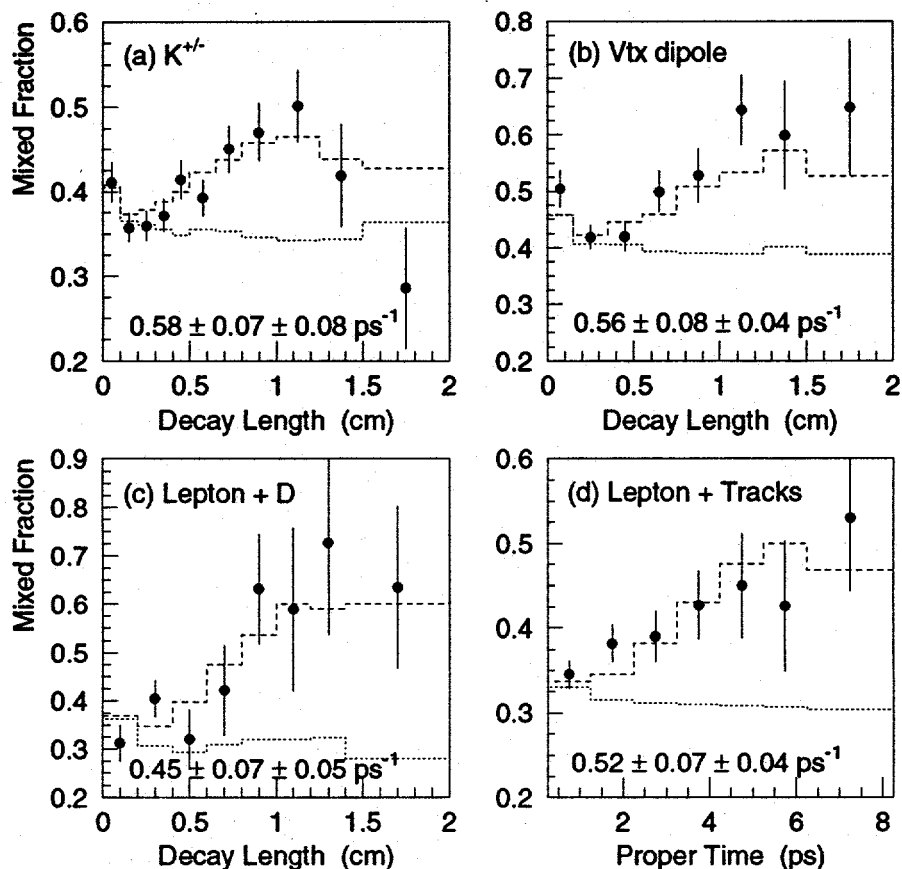
SLD Preliminary

Figure 17: Distributions of the fraction of decays tagged as mixed as a function of decay length or proper time for data (points) and best fit MC (dashed histograms) for the various analyses: (a) charged kaon, (b) charge dipole, (c) lepton + D, and (d) lepton + tracks. The dotted histograms correspond to MC distributions with no B_d^0-$\overline{B_d^0}$ mixing.

Analysis	Kaon	Dipole	Lept+D	Lept+Trks
Detector simulation	0.036	0.010	0.020	0.013
Physics modeling	0.048	0.027	0.024	0.032
Fit systematics	0.045	0.026	0.038	–
Total	0.075	0.039	0.049	0.035

Table 4: Systematic uncertainties for the different Δm_d measurements (in ps^{-1}).

This requirement also improves the probability of correctly assigning all of the B_d^0 decay tracks. The direction of the vertex axis is adjusted to minimize the impact parameter sum of the tracks in the vertex and the mean track impact parameter is required to be less than 50 μm at this minimum. A sample of 3291 decays satisfies the selection criteria. The "charge dipole" δq of the vertex is then defined as the relative displacement between the weighted mean location L_i of the positive tracks and of the negative tracks (see Sec. 1.6 for a definition of the quantity L): $\delta q = (\sum^+ w_i L_i)/(\sum^+ w_i) - (\sum^- w_i L_i)/(\sum^- w_i)$, where the first (second) term is a sum over all positive (negative) tracks in the vertex. The weight w_i for each track i is inversely proportional to the uncertainty on the quantity L_i, $w_i = \sin^2 \theta_i / \sigma_T$, with θ_i the angle between track i and the vertex axis and σ_T the uncertainty on the impact parameter of the track with respect to the vertex axis. Figure 18
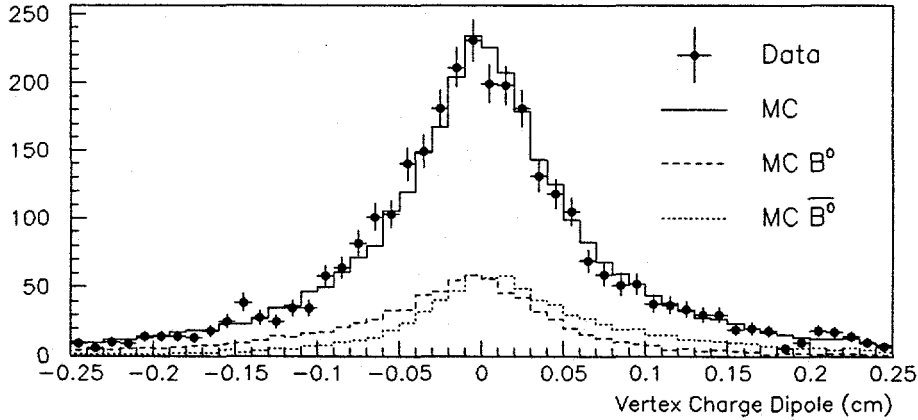
Figure 18: Distribution the vertex charge dipole for data (points) and MC (solid line). The contribution from MC B_d^0 and $\overline{B_d^0}$ decays is also indicated by the dashed and dotted histograms, respectively.

shows the distribution of the reconstructed charge dipole for data and MC. Also shown is the separation between B_d^0 and $\overline{B_d^0}$ decays. The correct tag probability increases with the magnitude of δq and reaches a maximum of 84% in the tails. This probability can be parameterized as $P_D = 0.84 \, e^{-|2.4|\delta q|-0.8|^3}$. A χ^2 fit to the mixed fraction distribution as a function of decay length [Fig. 17(b)] yields $\Delta m_d = 0.561 \pm 0.078(\text{stat}) \pm 0.039(\text{syst})$ ps^{-1} with a $\chi^2/\text{dof} = 8.8/7$. The main contributions to the systematic error come from MC statistics and fit systematics (see Table 4).

The next two analyses select semileptonic decays. The first of these (lep-

ton + D)[26] is identical to that used to measure the B^+ and B_d^0 lifetimes (see Sec. 2.1). As for the charge dipole analysis, a set of neutral vertices is selected. The sample here consists of 582 neutral decays with a B_d^0 purity of 61%. The charge of the lepton tags the $B_d^0/\overline{B_d^0}$ flavor at decay with a correct tag probability of 85%. As for the above two analyses, a χ^2 fit to the mixed fraction distribution [Fig. 17(c)] yields $\Delta m_d = 0.452 \pm 0.074(\text{stat}) \pm 0.049(\text{syst})$ ps^{-1} with a χ^2/dof $= 7.8/7$. The systematic error is dominated by MC statistics and fit systematics (see Table 4).

The last analysis (lepton+tracks)[27] selects semileptonic decays by identifying electrons and muons with high transverse momentum $p_T > 0.8$ GeV/c with respect to the nearest jet axis. This enhances the fraction of $Z^0 \to b\bar{b}$ events and allows for the use of a fully inclusive vertexing technique. The B decay vertex is estimated by computing an average intersection point between the lepton trajectory and all well-measured tracks in the jet, each track being weighted according to its probability to originate from the decay of a short-lived heavy hadron. This technique is very efficient ($\epsilon = 98\%$) once a high-p_T lepton has been selected and has good decay length resolution. Contrary to the first three analyses described above, the B decay proper time is reconstructed by estimating the B hadron momentum based on track and energy clusters in the calorimeter. The final sample contains 2609 semileptonic decay candidates with an estimated B hadron purity of 93%. The lepton charge provides the final state tag with correct tag probability of 85%.

For this analysis, the value of Δm_d is extracted from an unbinned maximum likelihood analysis with parameterizations estimated from the MC. The fit yields $\Delta m_d = 0.520 \pm 0.072(\text{stat}) \pm 0.035(\text{syst})$ ps^{-1} and the corresponding mixed fraction distribution is shown in Fig. 17(d). Main systematic uncertainties are presented in Table 4.

The results from the four analyses described above have been combined, taking into account statistical and systematic correlations between analyses, to produce the following SLD average for the mass difference between the two B_d^0 weak eigenstates:

$$\Delta m_d = 0.525 \pm 0.043(\text{stat}) \pm 0.037(\text{syst}) \text{ ps}^{-1}. \tag{42}$$

As expected, the statistical correlation coefficients are the largest between the kaon and charge dipole analyses, and between the two semileptonic analyses. The SLD average is compared with averages from other experiments in Fig. 19.
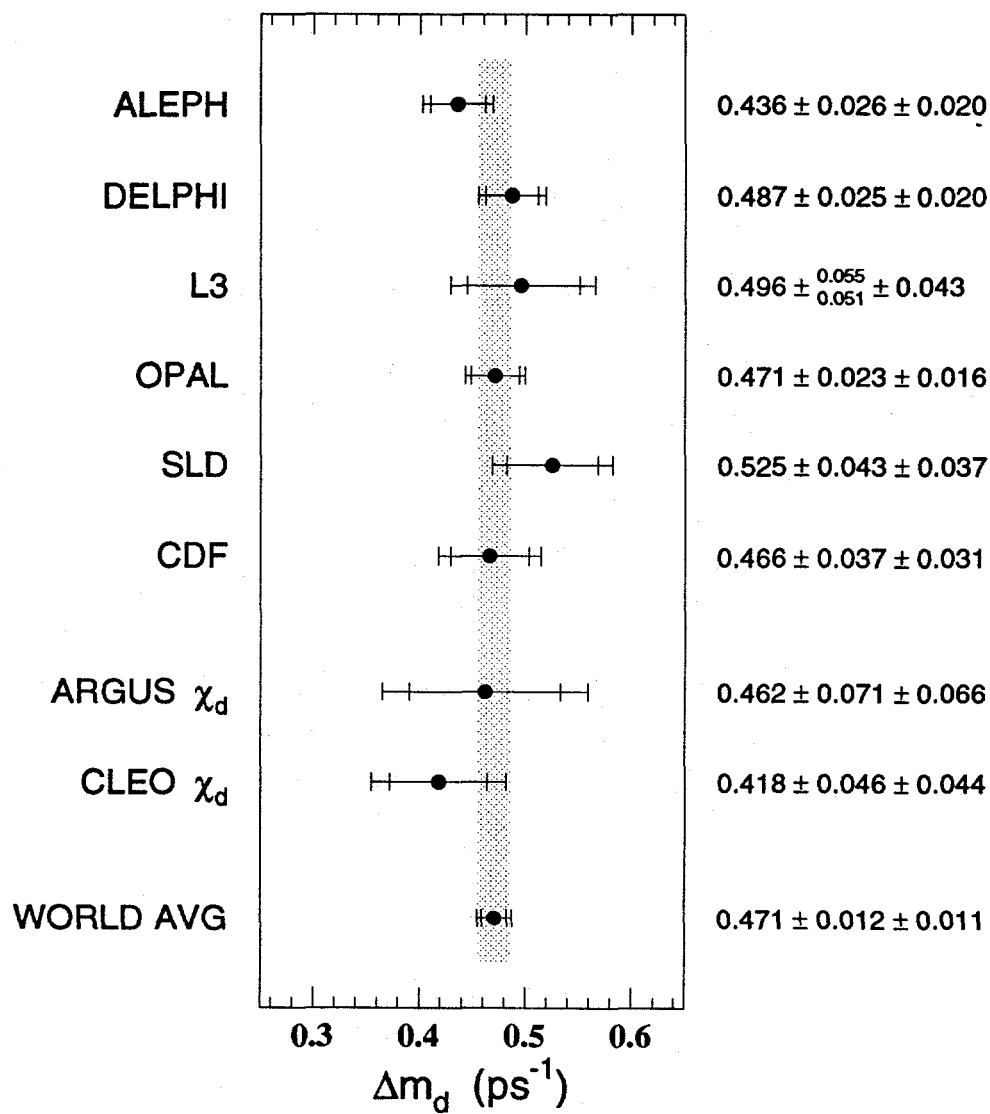
31

B$_d^0$ Mixing Δm_d Measurements

ALEPH	$0.436 \pm 0.026 \pm 0.020$
DELPHI	$0.487 \pm 0.025 \pm 0.020$
L3	$0.496 \pm ^{0.055}_{0.051} \pm 0.043$
OPAL	$0.471 \pm 0.023 \pm 0.016$
SLD	$0.525 \pm 0.043 \pm 0.037$
CDF	$0.466 \pm 0.037 \pm 0.031$
ARGUS χ_d	$0.462 \pm 0.071 \pm 0.066$
CLEO χ_d	$0.418 \pm 0.046 \pm 0.044$
WORLD AVG	$0.471 \pm 0.012 \pm 0.011$

Δm_d (ps^{-1})

Figure 19: Comparison between the various Δm_d measurements.

3   QCD Physics

Among the QCD analyses performed at SLD, we focus on those addressing the problem of hadronization — the process which turns an initial set of quarks into final state hadrons. Thanks to the unique SLC/SLD environment, quark fragmentation can be studied for differences between light-quark and heavy-quark fragmentation, as well as for differences between quark and antiquark fragmentation.

3.1   Charged Multiplicity in Light-, c-, and b-Quark Events

Perturbative QCD predicts that the difference in average charged multiplicity between heavy-quark Q and light-quark uds events $\Delta n_Q \equiv \bar{n}_Q - \bar{n}_{uds}$ is independent of center-of-mass energy. This prediction has been tested with a technique[28] following three steps: (i) the primary quark flavor is tagged in each event hemisphere, (ii) the number of charged tracks is counted in the opposite hemisphere to minimize the bias due to the quark flavor tag, (iii) the average charged multiplicity in each flavor-tagged sample is unfolded to correct for the purity and bias of the tags. The uds- (b-) tag requires that the hemisphere contains no track (at least three tracks) with signed 2-D impact parameter larger than $3\,\sigma$. Since the impact parameter tag provides a c quark sample of only modest purity, a more exclusive technique is used. For the c-quark tag, high-momentum charged D^* mesons are reconstructed in the $D^{*+} \rightarrow D^0\pi^+$, $D^0 \rightarrow K^-\pi^+$, and $D^0 \rightarrow K^-\pi^+(\pi^0)$ modes (the π^0 is not directly reconstructed), and charged D mesons are reconstructed in the $D^+ \rightarrow K^-\pi^+\pi^+$ mode. The number of uds-, c-, and b-tagged hemispheres is 154151, 976, and 9480 respectively with uds, c, and b purities estimated to be 75%, 64%, and 94% respectively.

After unfolding for the tag purities and (small) biases, we find the following multiplicity differences between c-quark and uds-quark, and between b-quark and uds-quark hemispheres:

$$\Delta n_c = 1.07 \pm 0.47(\text{stat})^{+0.36}_{-0.30}(\text{syst}), \tag{43}$$

$$\Delta n_b = 2.93 \pm 0.14(\text{stat})^{+0.30}_{-0.29}(\text{syst}). \tag{44}$$

The main contributions to the systematic errors arise from uncertainties in the detector acceptance and in the modeling of B hadron production and decay. These

results are compared with similar measurements performed at lower center-of-mass energies in Fig. 20. The data are consistent with the QCD prediction of energy
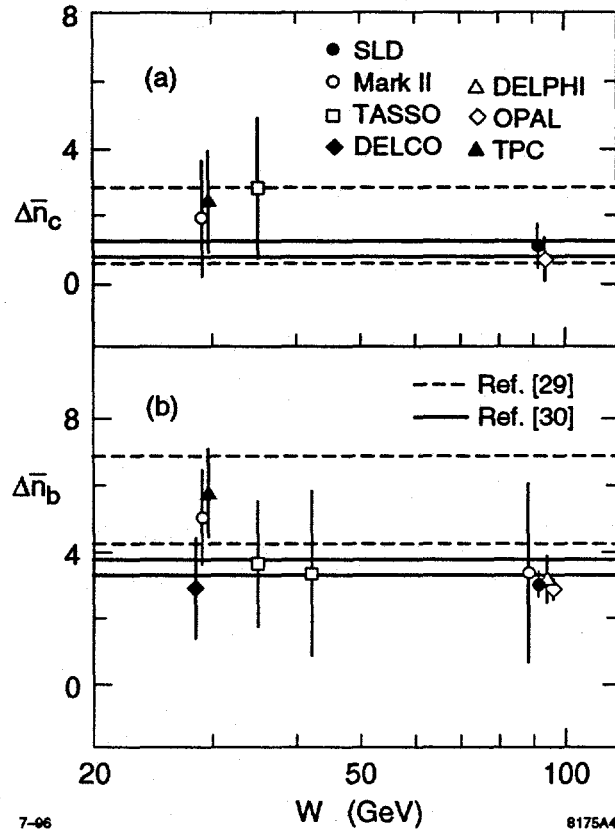

Figure 20: Multiplicity difference measurements as a function of center of mass energy for (a) c-quarks, and (b) b-quarks. Predictions from Refs.[29,30] are also indicated.

independence of Δn_Q over center-of-mass energies in the range between 29 and 91 GeV, and with absolute predictions.[29,30]

3.2 Identified Particle Production

Further knowledge about the fragmentation process can be gained by studying the production characteristics of different particle types.[31] Charged hadrons π, K, and p are identified with the CRID. Neutral hadrons are also selected: K_s^0 and Λ decays are identified via their two-prong decays, ϕ and K^{*0} are selected with identified charged kaons in the CRID.

Figure 21 shows the K^+K^- invariant mass distributions for ϕ decay candidates

34
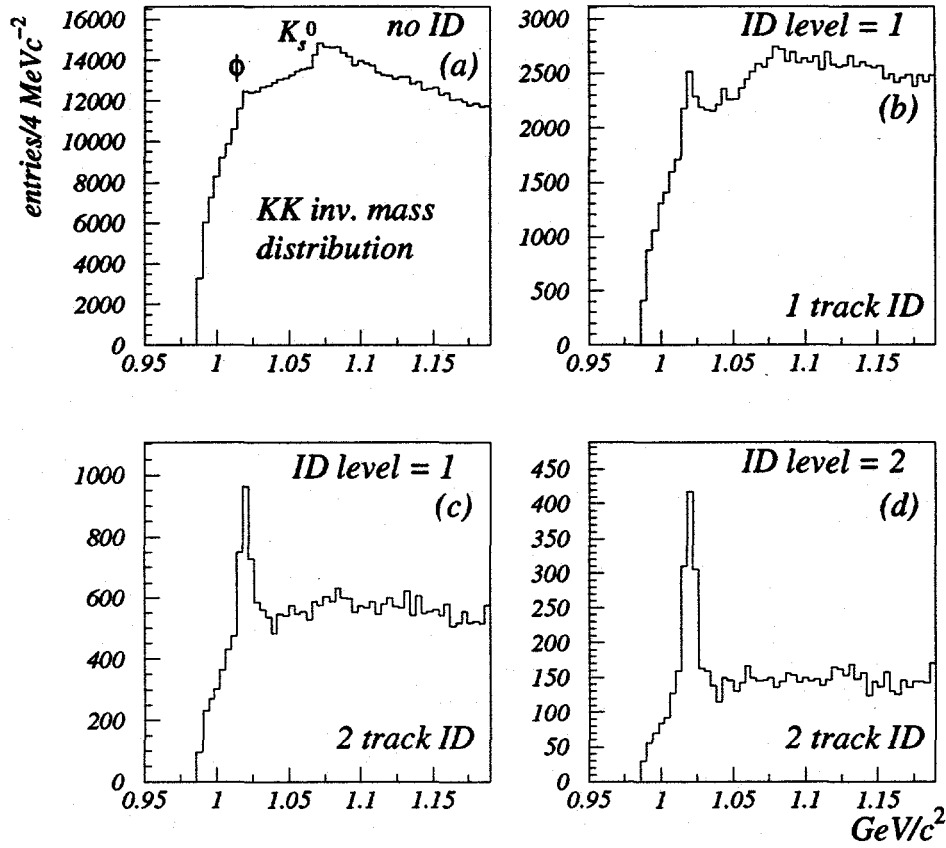
Figure 21: Invariant mass distributions for $\phi \to K^+ K^-$ decay candidates without and with various levels of kaon identification.

with increasingly tighter kaon identification requirements. It clearly demonstrates the power of the kaon identification. In order to measure the production rates, it is necessary to accurately determine the identification efficiency for each particle species. Charged particle identification efficiencies (and misidentification) are estimated primarily from pure data samples of charged pions from K_s^0 and τ decays, whereas proton samples are obtained from Λ decays. Efficiencies for neutral strange particles are estimated from the MC. The differential production rates for the above particle species are shown in Fig. 22 as a function of the scaled momentum variable $x_p = 2p/\sqrt{s}$. Suppression of particles containing strange valence quarks is clearly observed, with an even stronger suppression for ϕ mesons which contain an $s\bar{s}$ valence pair.

The production rates of $\pi^{\pm}$, $K^{\pm}$, K^0 ($\overline{K^0}$), p ($\overline{\text{p}}$), and Λ ($\overline{\Lambda}$) have also been measured separately in uds- and b-tagged samples. The uds and b flavor-tags

35

Hadronic Spectra in Z^0 Decays
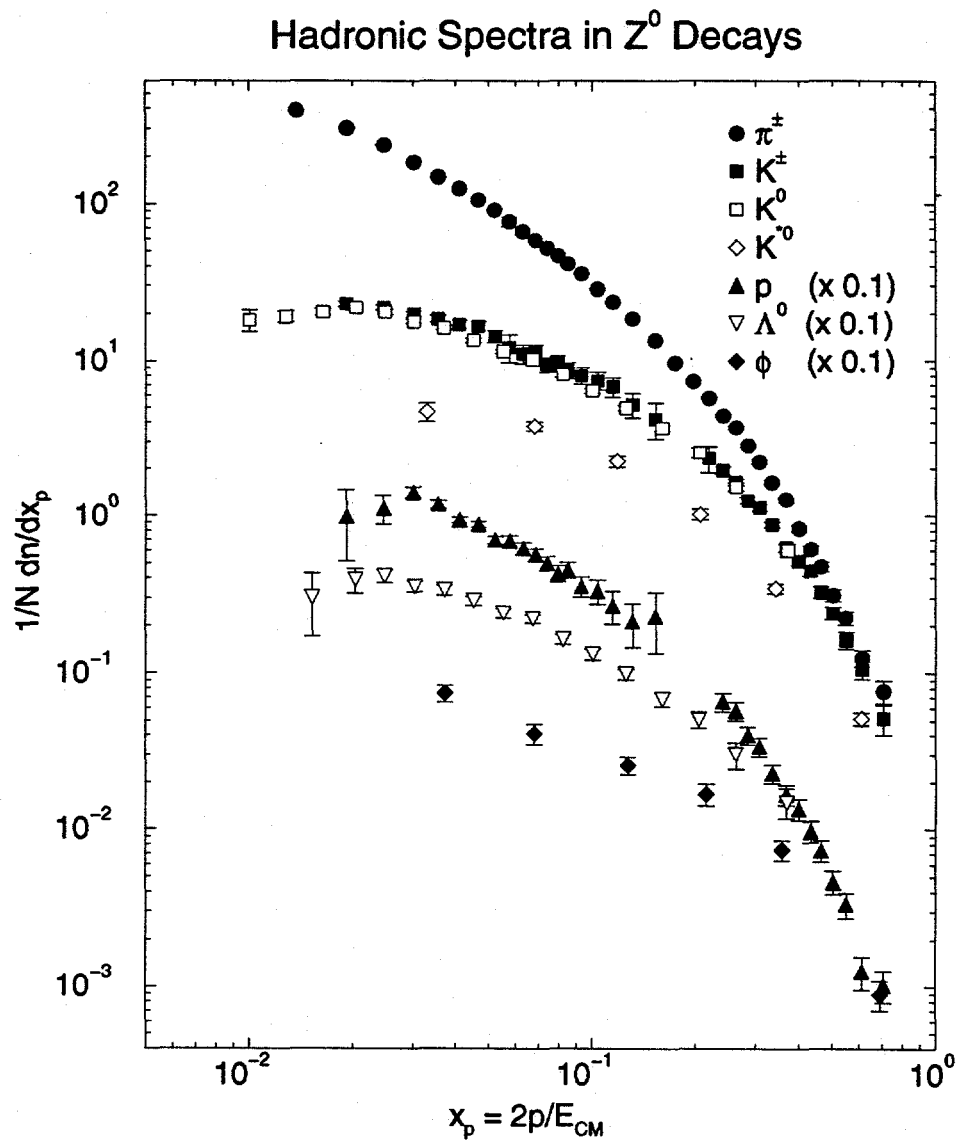
Figure 22: Differential production rates for identified particle species in hadronic Z^0 decays as a function of scaled momentum x_p.

are identical to the hemisphere tags described in the previous section except for being applied to the whole event. After unfolding for the tag purity (85% for *uds* and 89% for *b*) and bias, production rates in *uds*- and *b*-quark fragmentation are measured. This allows for a direct comparison of particle production in light- and heavy-quark hemispheres. The measured ratio between *b* and *uds* production of the various identified hadrons is shown in Fig. 23. This is the first such measure-
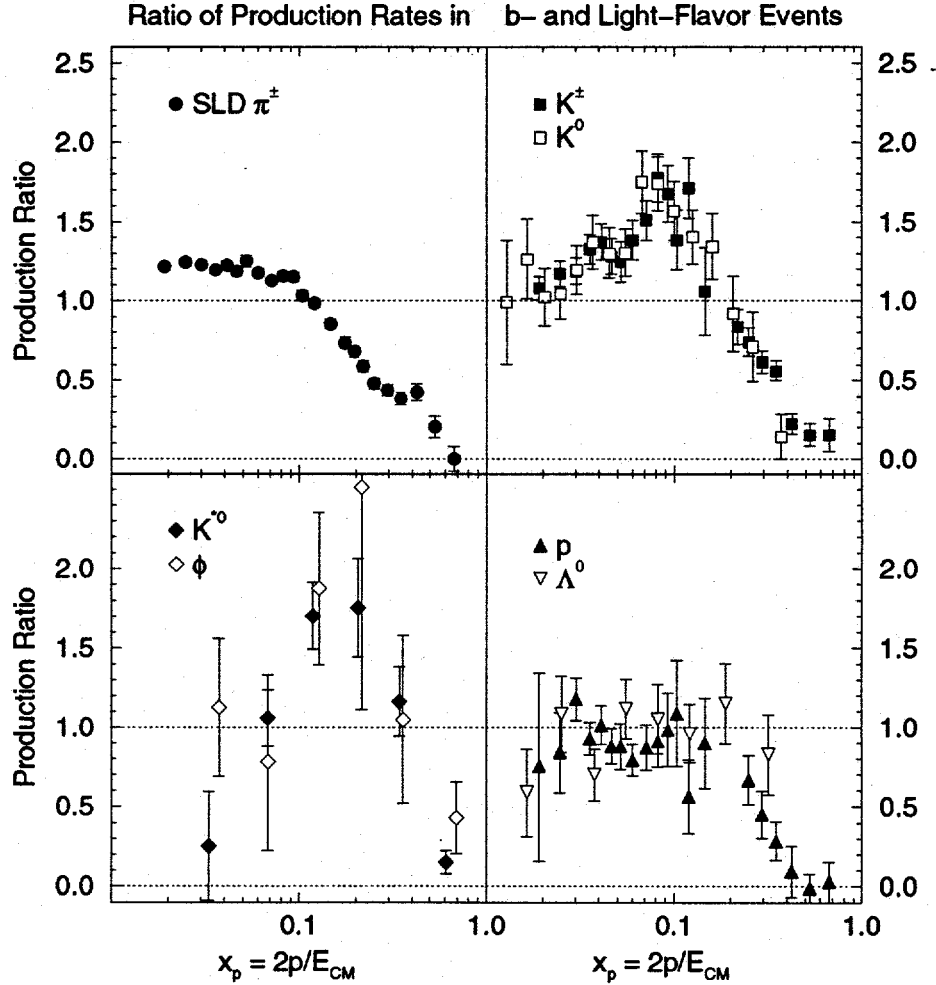
Figure 23: Ratio between the particle production rates in *b*-quark and *uds*-quark hemispheres as a function of scaled momentum for various particle species.

ment. Meson production is generally higher (lower) for *b* fragmentation at low (high) x_p, in agreement with the known characteristics of *B* hadron production and decay. Baryons are produced equally for $x_p < 0.15$ but are produced less

37

abundantly at larger x_p in b fragmentation. Statistical uncertainties in the ratio dominate because the dominant particle identification systematic uncertainties mostly cancel in the ratio. The measured production ratios agree well with the simulation based on JETSET 7.4.

3.3 Leading Particle Effect

Studies of charmed and B hadron production in $e^+e^- \to c\bar{c}$ and $e^+e^- \to b\bar{b}$ indicate that heavy quarks fragment into a single heavy hadron which carries a large fraction of the initial quark momentum. In that sense, there is ample evidence for "leading" particle production in e^+e^- interactions, where a leading particle is defined to be a particle which contains the primary q or $\bar{q}$. However, there is little evidence for leading particle production in light-quark fragmentation.

A unique technique is used to extract such evidence.[32] First, events are required to pass the uds-tag selection criteria described earlier. Then, the large polarized forward-backward asymmetry is exploited to tag quark and antiquark hemispheres in a way similar to that used for the B_d^0–$\overline{B_d^0}$ mixing measurements (see Sec. 2.2). A quark-tag purity of 73% is obtained for events with thrust axis $|\cos\theta_T| > 0.2$ for which the asymmetry is sufficiently large. The production rates of π^-, K^-, $\overline{K}^{*0}$, p, and Λ are measured separately in the quark- and antiquark-tagged hemispheres. A small contamination from heavy quarks in the uds-tagged event sample is subtracted and a correction is applied to account for the purity of the quark tag.

To compare the production rates $\mathcal{F}^h$ for a specific hadron h in quark and antiquark hemispheres, the normalized difference between these rates is computed: $D_h = (\mathcal{F}_q^h - \mathcal{F}_{\bar{q}}^h)/(\mathcal{F}_q^h + \mathcal{F}_{\bar{q}}^h)$. The distribution of D_h for the various identified hadrons as a function of scaled momentum is shown in Fig. 24. It is observed that more high-momentum protons or Λ's are produced than antiprotons or $\bar{\Lambda}$'s in quark hemispheres. This represents clear evidence for leading baryon production since protons and Λ's contain valence quarks, whereas their antiparticles do not. A higher production of high-momentum K^- and $\overline{K}^{*0}$ in quark hemispheres is also observed. Since mesons contain both valence quarks and antiquarks, one might expect to observe no effect. However, strangeness suppression makes it more likely for a $\overline{K}^{*0}$ (made of a $\bar{d}s$ valence pair) to contain a primary s quark than a primary $\bar{d}$ quark. Thus, the excess of $\overline{K}^{*0}$ over K^{*0} production in quark hemispheres, in-
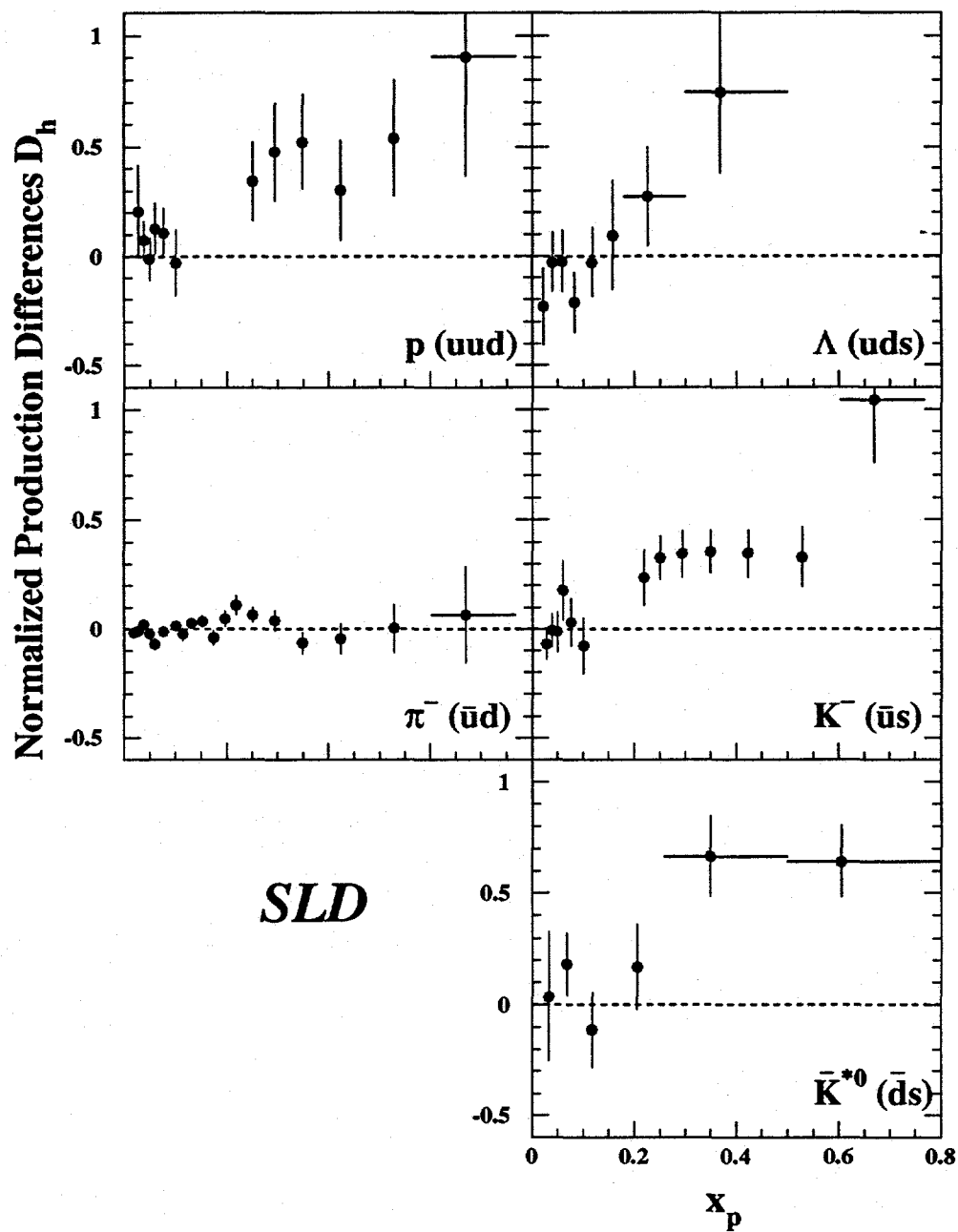
Figure 24: Normalized difference between production rates for a given hadron as a function of scaled momentum.

dicates both the existence of leading $\overline{K}^{*0}$ production and strangeness suppression at the highest momenta. Similarly, an excess of high-momentum K^- over K^+ is observed. There is no difference between π^- and π^+ production in quark hemispheres. The measured behavior measured in Fig. 24 is well-reproduced by the simulation with JETSET 7.4.

4 Summary and Future

Using a sample of $\sim 150,000$ hadronic Z^0 decays collected between 1993 and 1995, the SLD Collaboration has produced precise and/or unique tests of the Standard Model. These analyses take advantage of the large longitudinal electron beam polarization, the small and stable SLC beam spot, the high-resolution 3-D pixel vertex detector (VXD2), and the particle identification capabilities of the Cherenkov Ring Imaging Detector.

In 1996, SLD installed an improved CCD Vertex Detector (VXD3). As shown in Figs. 25 and 26, this detector is improved in many ways: (i) the angular coverage
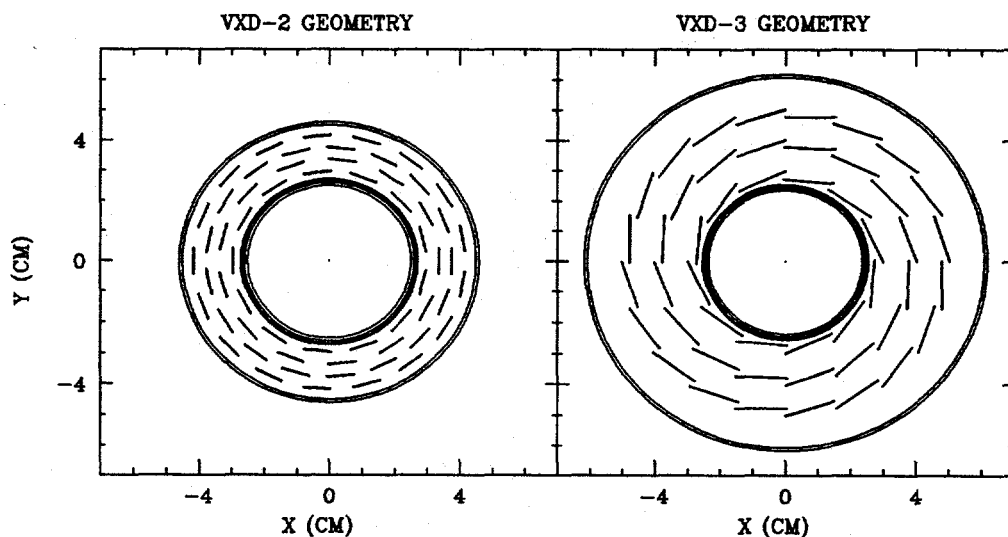
Figure 25: Cross-section views of the old (VXD2) and new (VXD3) vertex detectors.

is increased with maximum $|\cos\theta|$ of 0.90 instead of 0.74 for tracks with two hits; (ii) the average number of hits per track is increased from 2.3 to 3.2; (iii) the

VXD3

cosθ=0.85 ($\geqq$3 Hits)   cosθ=0.9 ($\geqq$2 Hits)

0   5   10
cm

cosθ=0.75 ($\geqq$2 Hits)
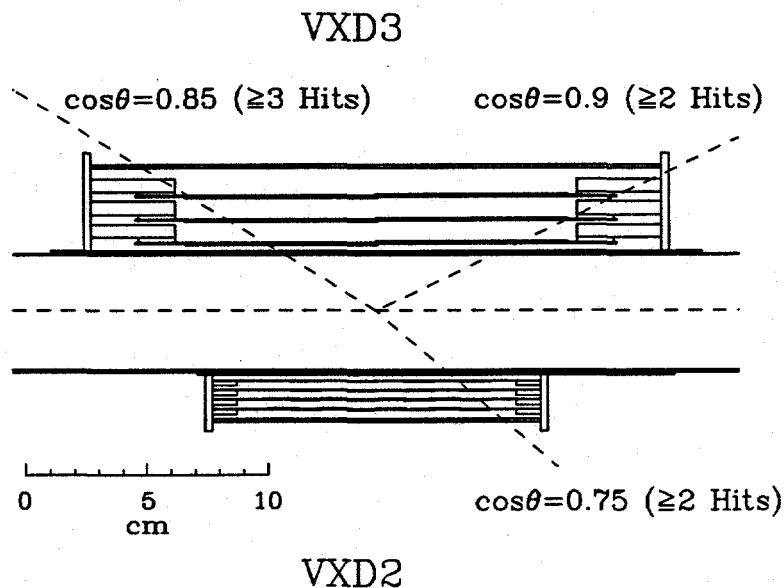
VXD2

Figure 26: Side-views of the old (VXD2) and new (VXD3) vertex detectors.

amount of material is reduced from 1.15% to 0.40% of a radiation length per ladder; (iv) the average distance between the inner and outer layer is increased from 12 to 20 mm to provide increased lever-arm. These features lead to significant improvements in resolution. In particular, the decay length resolution improves by roughly a factor of two.

Many measurements relying on precise tracking will benefit greatly from the increased resolution and coverage of VXD3. In particular, it is expected that the superior resolution will enable SLD to study the time dependence of B_s^0-$\overline{B_s^0}$ mixing up to very high oscillation frequencies, significantly increasing the reach in Δm_s currently attained by the LEP experiments.

Acknowledgments

References

[1] M. Woods, in *Proceedings of the AIP Conference*, Vol. 343 (1995), p. 230.

[2] E. Torrence, *Determination of Electroweak Parameters at the SLC*, SLAC-PUB-7307, September 1996, to appear in Proc. of ICHEP96, Warsaw, Poland, July 25-31, 1996.

[3] SLD Collab., K. Abe *et al.*, Phys. Rev. Lett. **70**, 2515 (1993).

[4] SLD Collab., K. Abe *et al.*, Phys. Rev. Lett. **73**, 25 (1994).

[5] SLD Collab., K. Abe *et al.*, *Measurement of the Z^0-Lepton Couplings Asymmetries A_l*, SLAC-PUB-7234, July 1996, contribution (PA07-063) to ICHEP96.

[6] SLD Collab., K. Abe *et al.*, Phys. Rev. Lett. **74**, 2880 (1995).

[7] SLD Collab., K. Abe *et al.*, Phys. Rev. Lett. **78**, 17 (1997).

[8] LEP Electroweak Working Group and SLD Heavy Flavor Group, *A Combination of Preliminary LEP and SLD Electroweak Measurements and Constraints on the Standard Model*, LEPEWWG/96-02, July 1996.

[9] C. J. S. Damerell *et al.*, Nucl. Instrum. Methods A **288**, 236 (1990).

[10] M. D. Hildreth *et al.*, IEEE Trans. Nucl. Sci. **42**, 451 (1994).

[11] SLD Collab., K. Abe *et al.*, Phys. Rev. D **53**, 1023 (1996).

[12] K. Abe *et al.*, Nucl. Instrum. Methods A **343**, 74 (1994).

[13] ARGUS Collab., H. Albrecht *et al.*, Z. Phys. C **62**, 371 (1994).

[14] SLD Collab., K. Abe *et al.*, *Measurement of A_b and A_c at the Z^0 Resonance Using a Lepton Tag*, SLAC-PUB-7233, July 1996, contribution (PA10-026) to ICHEP96.

[15] D. Axen *et al.*, Nucl. Instrum. Methods A **328**, 472 (1993).

[16] A. C. Benvenuti *et al.*, Nucl. Instrum. Methods A **290**, 353 (1990).

[17] SLD Collab., K. Abe *et al.*, Phys. Rev. Lett. **74**, 2895 (1995).

[18] D. Su, *Production of Charm and Beauty in e^+e^- with Polarized Electron Beam*, SLAC-PUB-7000, September 1995, *Proc. of 6th Int. Symp. on Heavy Flavor Physics*, Pisa, Italy, June 6-10, 1995.

[19] T. Takeuchi, A. Grant, and J. Rosner in *Proceedings of the 8th Meeting Division of Particles and Fields*, Albuquerque, August, 1994, Vol. 2, (World Scientific, New York, 1995), p. 1231.

[20] D. Jackson, Nucl. Instrum. Methods A **388**, 247 (1997).

[21] See, for example, I. I. Bigi *et al.*, in *B Decays*, edited by S. Stone (World Scientific, New York, 1994), p. 132.

[22] SLD Collab., K. Abe *et al.*, *Measurements of the B^+ and B^0 Lifetimes with Topological Vertexing at SLD*, SLAC-PUB-7227, July 1996, contribution (PA05-085) to ICHEP96.

[23] SLD Collab., K. Abe *et al.*, *Measurements of the B^+ and B^0 Lifetimes from the Semileptonic Decays at SLD*, SLAC-PUB-7226, July 1996, contribution (PA05-084) to ICHEP96.

[24] See, for example, L. K. Gibbons, *Status of Weak Quark Mixing* UR-1494, April 1997, to appear in *Proc. of ICHEP96*, Warsaw, Poland, July 25-31, 1996, and references therein.

[25] SLD Collab., K. Abe *et al.*, *Preliminary Measurements of the Time Dependence of $B_d^0 - \overline{B_d^0}$ Mixing with Kaon and Charge Dipole Tags*, SLAC-PUB-7230, July 1996, contribution (PA08-027/028) to ICHEP96.

[26] SLD Collab., K. Abe *et al.*, *Measurement of Time-dependent B_d^0–$\overline{B_d^0}$ Mixing Using Topology and Charge Selected Semi-Leptonic B Decays*, SLAC-PUB-7229, July 1996, contribution (PA08-026B) to ICHEP96.

[27] SLD Collab., K. Abe *et al.*, *Measurement of Time-Dependent B_d^0–$\overline{B_d^0}$ Mixing Using Inclusive Semileptonic Decays*, SLAC-PUB-7230, July 1996, contribution (PA08-026A) to ICHEP96.

[28] SLD Collab., K. Abe *et al.*, Phys. Lett. B **386**, 475 (1996).

[29] B. Schumm *et al.*, Phys. Rev. Lett. **69**, 3025 (1992).

[30] V. A. Petrov and A. V. Kisselev, Z. Phys. C **66**, 453 (1995).

[31] SLD Collab., M. Dima, SLAC-PUB-7199, June 1996, *Production of $\pi^\pm$, $K^\pm$, ρ, K_s^0, Λ^0, K^{*0} and ϕ in Hadronic Z^0 decays*, SLAC-PUB-7280, Aug. 1996, to appear in *Proc. of the 9th Meeting Division of Particles and Fields*, Minneapolis, Minnesota, Aug. 10-15, 1996.

[32] SLD Collab., K. Abe *et al.*, Phys. Rev. Lett. **78**, 3442 (1997).

**K. Abe,[19] K. Abe,[30] T. Akagi,[28] N.J. Allen,[4] W.W. Ash,[28]† D. Aston,[28]

K.G. Baird,[16] C. Baltay,[34] H.R. Band,[33] M.B. Barakat,[34] G. Baranko,[9] O. Bardon,[15]

T. L. Barklow,[28] G.L. Bashindzhagyan,[18] A.O. Bazarko,[10] R. Ben-David,[34]

A.C. Benvenuti,[2] G.M. Bilei,[22] D. Bisello,[21] G. Blaylock,[16] J.R. Bogart,[28] B. Bolen,[17]

T. Bolton,[10] G.R. Bower,[28] J.E. Brau,[20] M. Breidenbach,[28] W.M. Bugg,[29]

D. Burke,[28] T.H. Burnett,[32] P.N. Burrows,[15] W. Busza,[15] A. Calcaterra,[12]

D.O. Caldwell,[5] D. Calloway,[28] B. Camanzi,[11] M. Carpinelli,[23] R. Cassell,[28]

R. Castaldi,[23](a) A. Castro,[21] M. Cavalli-Sforza,[6] A. Chou,[28] E. Church,[32]

H.O. Cohn,[29] J.A. Coller,[3] V. Cook,[32] R. Cotton,[4] R.F. Cowan,[15] D.G. Coyne,[6]

G. Crawford,[28] A. D'Oliveira,[7] C.J.S. Damerell,[25] M. Daoudi,[28] R. De Sangro,[12]

R. Dell'Orso,[23] P.J. Dervan,[4] M. Dima,[8] D.N. Dong,[15] P.Y.C. Du,[29] R. Dubois,[28]

B.I. Eisenstein,[13] R. Elia,[28] E. Etzion,[33] S. Fahey,[9] D. Falciai,[22] C. Fan,[9]

J.P. Fernandez,[6] M.J. Fero,[15] R. Frey,[20] K. Furuno,[20] T. Gillman,[25] G. Gladding,[13]

S. Gonzalez,[15] E.L. Hart,[29] J.L. Harton,[8] A. Hasan,[4] Y. Hasegawa,[30] K. Hasuko,[30]

S. J. Hedges,[3] S.S. Hertzbach,[16] M.D. Hildreth,[28] J. Huber,[20] M.E. Huffer,[28]

E.W. Hughes,[28] H. Hwang,[20] Y. Iwasaki,[30] D.J. Jackson,[25] P. Jacques,[24]

J. A. Jaros,[28] A.S. Johnson,[3] J.R. Johnson,[33] R.A. Johnson,[7] T. Junk,[28]

R. Kajikawa,[19] M. Kalelkar,[24] H. J. Kang,[26] I. Karliner,[13] H. Kawahara,[28]

H.W. Kendall,[15] Y. D. Kim,[26] M.E. King,[28] R. King,[28] R.R. Kofler,[16] N.M. Krishna,[9]

R.S. Kroeger,[17] J.F. Labs,[28] M. Langston,[20] A. Lath,[15] J.A. Lauber,[9]

D.W.G.S. Leith,[28] V. Lia,[15] M.X. Liu,[34] X. Liu,[6] M. Loreti,[21] A. Lu,[5] H.L. Lynch,[28]

J. Ma,[32] G. Mancinelli,[22] S. Manly,[34] G. Mantovani,[22] T.W. Markiewicz,[28]

T. Maruyama,[28] H. Masuda,[28] E. Mazzucato,[11] A.K. McKemey,[4] B.T. Meadows,[7]

R. Messner,[28] P.M. Mockett,[32] K.C. Moffeit,[28] T.B. Moore,[34] D. Muller,[28]

T. Nagamine,[28] S. Narita,[30] U. Nauenberg,[9] H. Neal,[28] M. Nussbaum,[7] Y. Ohnishi,[19]

L.S. Osborne,[15] R.S. Panvini,[31] C.H. Park,[27] H. Park,[20] T.J. Pavel,[28] I. Peruzzi,[12](b)

M. Piccolo,[12] L. Piemontese,[11] E. Pieroni,[23] K.T. Pitts,[20] R.J. Plano,[24] R. Prepost,[33]

C.Y. Prescott,[28] G.D. Punkar,[28] J. Quigley,[15] B.N. Ratcliff,[28] T.W. Reeves,[31]

J. Reidy,[17] P.L. Reinertsen,[6] P.E. Rensing,[28] L.S. Rochester,[28] P.C. Rowson,[10]

J.J. Russell,[28] O.H. Saxton,[28] T. Schalk,[6] R.H. Schindler,[28] B.A. Schumm,[6] S. Sen,[34]

V.V. Serbo,[33] M.H. Shaevitz,[10] J.T. Shank,[3] G. Shapiro,[14] D.J. Sherden,[28]

K.D. Shmakov,[29] C. Simopoulos,[28] N.B. Sinev,[20] S.R. Smith,[28] M.B. Smy,[8]

J.A. Snyder,[34] P. Stamer,[24] H. Steiner,[14] R. Steiner,[1] M.G. Strauss,[16] D. Su,[28]

F. Suekane,[30] A. Sugiyama,[19] S. Suzuki,[19] M. Swartz,[28] A. Szumilo,[32]

T. Takahashi,[28] F.E. Taylor,[15] E. Torrence,[15] A.I. Trandafir,[16] J.D. Turk,[34]

T. Usher,[28] J. Va'vra,[28] C. Vannini,[23] E. Vella,[28] J.P. Venuti,[31] R. Verdier,[15]

P.G. Verdini,[23] D.L. Wagner,[9] S.R. Wagner,[28] A.P. Waite,[28] S.J. Watts,[4]

A.W. Weidemann,[29] E.R. Weiss,[32] J.S. Whitaker,[3] S.L. White,[29] F.J. Wickens,[25]

D.A. Williams,[6] D.C. Williams,[15] S.H. Williams,[28] S. Willocq,[28] R.J. Wilson,[8]

W.J. Wisniewski,[28] M. Woods,[28] G.B. Word,[24] J. Wyss,[21] R.K. Yamamoto,[15]

J.M. Yamartino,[15] X. Yang,[20] J. Yashima,[30] S.J. Yellin,[5] C.C. Young,[28] H. Yuta,[30]

G. Zapalac,[33] R.W. Zdarko,[28] and J. Zhou,[20]**

(The SLD Collaboration)

[1]Adelphi University, Garden City, New York 11530
[2]INFN Sezione di Bologna, I-40126 Bologna, Italy
[3]Boston University, Boston, Massachusetts 02215
[4]Brunel University, Uxbridge, Middlesex UB8 3PH, United Kingdom
[5]University of California at Santa Barbara, Santa Barbara, California 93106
[6]University of California at Santa Cruz, Santa Cruz, California 95064
[7]University of Cincinnati, Cincinnati, Ohio 45221
[8]Colorado State University, Fort Collins, Colorado 80523
[9]University of Colorado, Boulder, Colorado 80309
[10]Columbia University, New York, New York 10027
[11]INFN Sezione di Ferrara and Università di Ferrara, I-44100 Ferrara, Italy
[12]INFN Lab. Nazionali di Frascati, I-00044 Frascati, Italy
[13]University of Illinois, Urbana, Illinois 61801
[14]Lawrence Berkeley Laboratory, University of California, Berkeley, California 94720
[15]Massachusetts Institute of Technology, Cambridge, Massachusetts 02139
[16]University of Massachusetts, Amherst, Massachusetts 01003
[17]University of Mississippi, University, Mississippi 38677
[18]Moscow State University, Institute of Nuclear Physics 119899 Moscow, Russia
[19]Nagoya University, Chikusa-ku, Nagoya 464 Japan
[20]University of Oregon, Eugene, Oregon 97403
[21]INFN Sezione di Padova and Università di Padova, I-35100 Padova, Italy
[22]INFN Sezione di Perugia and Università di Perugia, I-06100 Perugia, Italy
[23]INFN Sezione di Pisa and Università di Pisa, I-56100 Pisa, Italy
[24]Rutgers University, Piscataway, New Jersey 08855
[25]Rutherford Appleton Laboratory, Chilton, Didcot, Oxon OX11 0QX United Kingdom
[26]Sogang University, Seoul, Korea
[27]Soongsil University, Seoul, Korea 156-743
[28]Stanford Linear Accelerator Center, Stanford University, Stanford, California 94309
[29]University of Tennessee, Knoxville, Tennessee 37996
[30]Tohoku University, Sendai 980 Japan
[31]Vanderbilt University, Nashville, Tennessee 37235
[32]University of Washington, Seattle, Washington 98195
[33]University of Wisconsin, Madison, Wisconsin 53706
[34]Yale University, New Haven, Connecticut 06511
†Deceased
[a]Also at the Università di Genova
[b]Also at the Università di Perugia

45